Comprehensive Summaries of Uppsala Dissertations
from the Faculty of Science and Technology 757

AlN and High-*k* Thin Films for IC and Electroacoustic Applications

BY

FREDRIK ENGELMARK

ACTA UNIVERSITATIS UPSALIENSIS
UPPSALA 2002

AlN and High-*k* Thin Films for IC and Electroacoustic Applications

BY

FREDRIK ENGELMARK

Dissertation for the Degree of Doctor of Philosophy in Solid State Electronics presented at Uppsala University in 2002

ABSTRACT

Engelmark, F. 2002. AlN and High-*k* Thin Films for IC and Electroacoustic Applications. Acta Universitatis Upsaliensis. *Comprehensive Summaries of Uppsala Dissertations from the Faculty of Science and Technology* 757. 80 pp. Uppsala. ISBN 91-554-5421-6

The explosive development of personal communications systems, navigation, satellite communications as well as personal computer and data processing systems together with the constant demand for higher speeds and larger bandwidths has driven the fabrication technology to its limits. This in turn necessitates the development of novel functional materials for the fabrication of devices with superior performance and higher capacity at reduced manufacturing costs. This thesis focuses on the synthesis and characterization of such materials for IC and electroacoustic applications. Specifically, AlN thin films as well as Ti doped Ta_2O_5 thin films have been grown using both RF and pulsed-DC reactive sputter deposition on a variety of substrate materials. AlN is a piezoelectric material and hence its crystallographic structure and film texture are of prime interest, while Ta_2O_5 is a material with a relatively high dielectric constant. A significant part of the work deals with the optimization of the deposition processes. The latter have been optimized both empirically and theoretically by modeling the reactive sputter process. Subsequently, highly textured AlN thin films have been synthesized and characterized. The films were fully c-axis oriented with a typical value for the FWHM of the (002) rocking curve of 1.6°. In addition, epitaxial AlN films have been grown on sapphire at 500^{o}C with relatively low defect density.

Further, a highly selective dry etch process for etching Al on AlN has been developed for the fabrication of MIM, MIS, SAW and BAW test structures for electrical and electroacoustic characterization of the films. A dielectric constant of 10 for AlN and 25 for Ti doped Ta_2O_5 have been measured. With respect to electroacoustic characterization, BAW measurements gave a longitudinal velocity of 11350 m/s and a TCD of -25ppm/K. AlN thin film test structures on SiO_2/Si yielded a SAW velocity of around 5000 m/s, while those on polycrystalline diamond exhibited a SAW velocity of 11800 m/s. The latter results illustrate one of the biggest advantages of thin film SAW technology, namely one can exploit both the piezoelectric properties of the film and the acoustic properties of the substrate and hence devise components with superior performance.

Fredrik Engelmark, Solid State Electronics, The Ångström Laboratory
Uppsala University, Box 534, SE-751 21 Uppsala, Sweden

ISSN 1104-232X
ISBN 91-554-5421-6

Printed in Sweden by Reklam & Katalogtryck, Uppsala 2002

Publications

This thesis is based on the following publications, which in the following will be referred to in the text by their Roman numerals.

I F. Engelmark, G. Fuentes, I. V. Katardjiev, A. Hårsta, U. Smith, and S. Berg, ”Synthesis of Highly Oriented Piezoelectric AlN Films by Reactive Sputter Deposition”, J. Vac. Sci. Technol. A **18**(4), Jul/Aug (2000) 1609-12

II L. B. Jonsson, J. Westlinder, F. Engelmark, C. Hedlund, J. Du, U. Smith, and H. -O. Blom, ”Patterning of Tantalum Pentoxide, a High Epsilon Material, by Inductively Coupled Plasma Etching”, J. Vac. Sci. Technol. B **18**(4), Jul/Aug (2000) 1906-10

III F. Engelmark, G. F. Iriarte, I. V. Katardjiev, M. Ottosson, P. Muralt, and S. Berg, “Structural and Electroacoustic Studies of AlN Thin Films During Low Temperature Radio Frequency Sputter Deposition”, J. Vac. Sci. Technol. A **19**(5), (2001) 2664-9

IV F. Engelmark, G. F. Iriarte, and I. V. Katardjiev, “Selective Etching of Al/AlN Structures for Metallization of Surface Acoustic Wave Devices” J. Vac. Sci. Technol. B **20**(3), (2002) 843-8

V G. F. Iriarte, F. Engelmark, and I. V. Katardjiev, ”Reactive Sputter Deposition of Highly Oriented AlN Films at Room Temperature” J. Mat. Res. **17**(6), (2002) 1469-75

VI F. Engelmark, J. Westlinder, T. Nyberg, and S. Berg, ”Experimental and Computer Simulation Studies of the ‘Baffled Target’ Reactive Sputtering Process” Submitted to J. Vac. Sci. Technol.

VII J. Westlinder, Y. Zhang, F. Engelmark, G. Possnert, H. -O. Blom, J. Olsson, and S. Berg, “Simulation and Dielectric Characterization of Reactive DC Magnetron Cosputtered $(Ta_2O_5)_{1-x}(TiO_2)_x$ Thin Films” J. Vac. Sci. Technol. B **20**(3), (2002) 855-61

VIII F. Engelmark, J. Westlinder, G. F. Iriarte, I. V. Katardjiev, J. Olsson, “Electrical Characterization of AlN MIS- and MIM-structures“ Submitted to IEEE – Transactions on Electron Devices

IX G. F. Iriarte, F. Engelmark, M. Ottosson, I. V. Katardjiev, “The Influence of the Deposition Parameters on the Stress of Magnetron Sputter Deposited AlN Thin Films on Si (100) Substrates” Submitted to Journal of Materials Research

Contents

1 Introduction

Acoustic wave devices based on piezoelectric materials have been in commercial use for over 60 years [1]. They are used in a wide variety of application such as delay lines, oscillators, resonators, sensors, actuators, dispersive delay lines, acoustic microscopy as well as in specialized military equipment. Nevertheless, by far the largest market is the telecommunication industry, primarily for wireless communication in mobile cell phones and base stations. This industry consumes approximately three billion acoustic wave filters for frequency control. The filters are typically based on surface acoustic wave (SAW) and bulk acoustic wave (BAW) resonator technology. Commonly used piezoelectric materials in SAW devices are single crystalline substrates of quartz (SiO_2), lithium tantalate ($LiTaO_3$) and lithium niobate ($LiNbO_3$). Other well-established resonator technologies are standard on chip LC, transmission lines, and ceramic resonators.

Recently, the enormous growth in personal communications systems (PCS) and navigation, satellite communication and various other forms of wireless data communication have made analogue frequency control a key issue, especially as the frequency spectrum crowding increases as well as the operation frequency increases to the microwave region. Also, the technological drive to minimize and improve the capacity of such systems has shown the need for the development of high performance, miniature, on chip filters operating in the low and medium GHz frequency range. At the frequency of interests, other resonator technologies such as LC, ceramic resonators and transmission line resonators become too large for wireless applications [2].

One of the biggest disadvantages of the standard electroacoustic technology in the microwave region is that it makes use of single crystalline piezoelectric materials, the choice of which is rather limited and which by definition are incompatible with the IC-technology. In addition, the properties of these materials determine uniquely the acoustic velocity, which in turn together with the device dimensions define the operating frequency. Thus, the only way to increase the latter is to decrease the device dimensions which comes at an enormous increase in the fabrication costs, both for BAW and SAW devices particularly in the microwave region. In recent years thin piezoelectric films have been developed to extend electromechanical SAW and BAW devices to much higher frequencies [3, 4]. The standard bulk technology, however, continues and will continue to dominate the market for devices operating, say, less than 1 GHz.

For higher frequencies up to 20 GHz, on the other hand, Thin Film Bulk Acoustic Resonators (TFBAR or FBAR) is considered to be the most promising approach today because they are characterized with small dimensions, low losses, high power handling capabilities and not the least low fabrication cost. In addition, this approach allows the great flexibility of choosing at will the substrate/film combination, thus making use of the electroacoustic properties of the non piezoelectric substrate and widening greatly the choice of fabrication materials. Agilent Technologies [5] is the first company to start mass production of FBAR devices in Q1 2001. It should be strongly pointed out, however, that by far the

greatest potential of using thin films for the fabrication of TFBAR's is that it opens the very promising possibility of integrating the traditionally incompatible IC and electroacoustic technologies. This in turn will bring about a number of substantial benefits such as significant decrease in the fabrication cost of the final device, easier and simpler device design, reduced losses, increased sensitivity, reduced power consumption, reduced device size, reduced materials use, reduced electromagnetic contamination, etc.

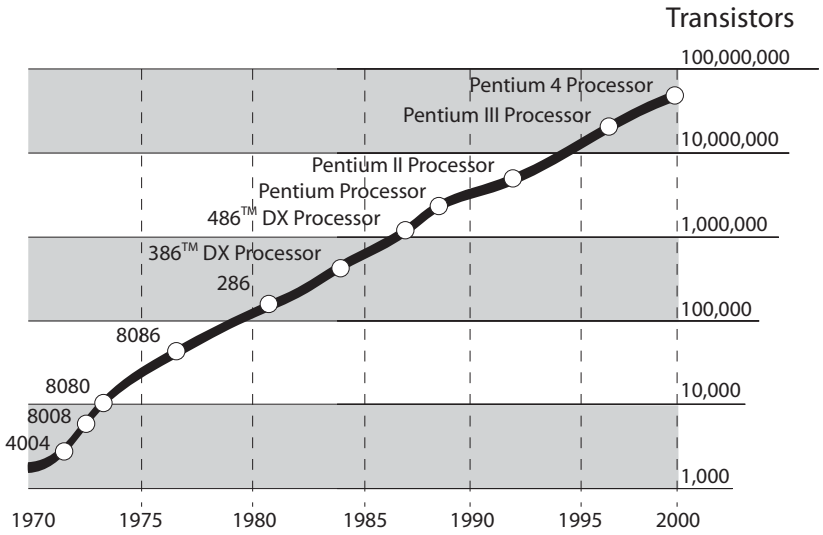

Figure 1. Moore's law has predicted the rapid development of MOS transistor technology since he first observed the "doubling of transistor density on a manufactured die every year" in 1965.

Thus, the research in this field is centered around the development of novel functional materials (piezoelectric, ferroelectric, etc.) with superior electroacoustic properties allowing the fabrication of high frequency devices with improved performance and at the same time at low fabrication cost. By the way of example, materials with high piezoelectric coefficients are sought to allow the design of bandpass filters with large bandwidths, say of the order of 10% or more. Further, these materials should exhibit low electroacoustic losses, i.e. should be characterized with a high quality factor as well as high thermal stability in the temperature range of operation. Tunability is also a desirable property. Not the least, the synthesis process should be compliant with the planar technology, while the materials themselves should be compatible with the IC-technology.

One major part of this thesis focuses on the synthesis and the characterization of one such material, namely AlN for electroacoustic applications. A particular attention is devoted to the development of a low temperature deposition process in view of an eventual integration of this technology with IC-fabrication due to thermal budget limitations. The synthesis process is further optimized in view of film texture, stress, density, surface roughness, etc. as well as electroacoustic

properties. In addition, processing steps such as lithography, metallization, etching, etc. have been developed for the fabrication of electroacoustic test structures and devices. Finally, capacitors, delay lines, electroacoustic resonators, and filters have been fabricated and evaluated.

In another but very closely related dimension the semiconductor industry has been developing at a remarkable pace over the last several decades. The number of transistors per unit area in an integrated circuit is doubled every 18:th month, according to Moore's law shown in Figure 1, and it is now debatable how much longer it is possible to sustain this rate. The performance of individual components is also increasing very fast, and the speed of the latter is doubled almost every year (MOS technology). As the competition intensifies between the dominating manufacturers to develop the fastest, most sophisticated circuit, the search for new materials tailored for specific applications goes on hand in hand with this development. Right now, a world wide effort is devoted to developing the next dielectric material in MOS gates, which will replace SiO_2 after some successful 40 years of reign, since the first MOSFET entered the scene in the 1960's [6]. The problem is that SiO_2 has a relatively low dielectric constant resulting in a steep decrease of the thickness of the gate oxide. The thickness of the gate oxide today is only a few atomic layers thick, and a further reduction is not realistic. The possible successors, compound oxides and nitrides like Al_2O_3, HfO_2, ZrO_2, Ta_2O_5 and AlN all have higher dielectric numbers than SiO_2, thus factors like process compatibility and power handling will determine the winner. Focus is also set on tailoring a certain process to enable the use of the best inherently suited material for a specific application. A famous example in that sense is the transition from Al to Cu as the metal interconnecting layer in IC-fabrication.

A smaller part of this thesis deals with process development and the synthesis of one such material, namely Ta_2O_5. The latter has also been doped with Ti to improve its properties. Post processing and electrical characterization of the films have also been performed.

1.1 Acoustic Wave Devices

Surface acoustic waves (SAW) in solids were first discovered at the beginning of the 19th century by lord Rayleigh. This type of waves is often referred to as Rayleigh waves, after their discoverer, and is a two dimensional wave confined to the surface of the solid to a depth of approximately two wavelengths. Owing to the much lower velocity of both SAW and BAW waves (more than 100,000 times slower than the speed of light) a wide variety of compact electro and opto acoustic devices, such as delay lines, convolvers, sensors, actuators, resonators, filters, etc. can be fabricated.

Acoustic waves in solids can be excited in a variety of ways, but by far the most popular method is the use of the piezoelectric effect exhibited by several classes of materials. Piezoelectricity actually means "pressing" electricity [7], indicating that by applying a mechanical pressure to this group of materials, a measurable potential difference develops between the two ends. Piezoelectricity was first discovered by Pierre Curie and his brother Paul-Jacques in 1880, and they also together discovered the inverse effect one year later. The phenomena is

responsible for the conversion of electric energy to acoustic energy, i.e. creating a wave propagating in the material, and also the possibility to convert it the other way around. That is, by applying a voltage to the material, it is also possible to achieve a slight dimensional variation. This can e.g. be used where a very accurate mechanical movement at the nanometer scale is desirable.

Acoustic wave devices operate generally but not exclusively on the following principle. An acoustic wave is normally excited in a solid by a so-called transducer. The wave is then guided to propagate in an acoustic cavity and finally the wave is detected by another transducer and subsequently analyzed. Thus for example, the wave propagation is a very sensitive function of the properties of the acoustic cavity, which in turn is an equally sensitive function of the ambient, allowing the fabrication of a wide variety of sensors (temperature, pressure, torque, acceleration, chemical, biological, etc.). Further, wave propagation in a cavity is dispersive, giving rise to complex resonant impedance characteristics, which allows the construction of resonators, oscillators, filters, etc. Thus the list of applications is indeed long.

Electroacoustic wave devices are traditionally fabricated on piezoelectric substrates such as $LiNbO_3$, $KNbO_3$, $BaTiO_3$, $Pb(Zr_xTi_{1-x})O_3$ among others. These crystals belong to the perovskite family, which are ferroelectric materials and hence exhibit the piezoelectric effect. The substrate is generally a single crystalline material, thus rather expensive since the manufacturing process is very complex and time consuming. Fabricating acoustic wave devices as discrete components also entails other problems. The device has to be connected to the rest of the electronics in some way, which is usually done by soldering, that is very time consuming. In addition, each interface between the electronic components is a source of power loss, and degrades the performance of the complete device. In addition, the electroacoustic and other properties of the above materials impose serious limitations on the performance of the devices, particularly at high frequencies which necessitates the development of new materials with improved properties. A natural development, which has attracted substantial interest in recent years, is the use of the thin film technology for the synthesis of new piezoelectric materials, which simultaneously opens the way for integration of the traditionally incompatible SAW/BAW and IC-technologies.

1.2 Thin film Acoustic Wave Devices

Synthesis of thin films necessitates the use of a supporting substrate. This brings along a wide range of advantages as well as provides great flexibility to the thin film electroacoustic technology as follows. Very often the acoustic cavity includes in part or in whole the substrate which means that one can tailor at will the electroacoustic and other properties of the devices by choosing a suitable piezo material/substrate combination. Thus for example, by choosing a substrate with higher SAW velocity one can increase the frequency of operation of SAW devices for one and the same lithographic resolution [8]. The quality factor of the device can also be improved in a similar way. Further, by choosing a substrate with opposite temperature coefficient of delay (TCD) one can devise a resonator with thermal stability rivaling that of quartz [9], etc. Finally, the use of thin films means

that such a process can be easily integrated with the planar technology. This enables the possibility of fabricating thin film SAW/BAW (FSAW/FBAW) components on chip, as just another step in the IC-processing line. Both SAW and BAW devices can be fabricated using this method, and choosing an IC-compatible combination of materials makes it possible to bring microelectronics and acoustic wave devices together in an efficient way. By way of example, Figure 2 shows a sketch of a thin film transversal SAW filter fabricated on a Si substrate with a SiO_2 interfacial layer for thermal compensation. In Figure 3, a membrane type BAW is illustrated. The buried bottom electrode complicates the fabrication of such a device as compared to SAW, which is discussed in great detail later in this thesis.

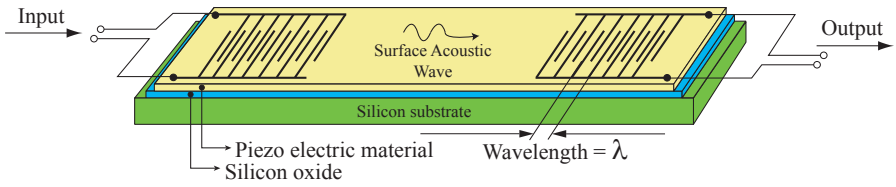

Figure 2. A transversal SAW filter structure. This type of SAW filter is relatively easy to fabricate, although it suffers from rather large loss due to its bi-directional nature.

Historically, ZnO was the first material for use in thin film acoustic wave devices [4], although it is gradually being phased out by e.g. aluminum nitride (AlN). Both ZnO and AlN have a wurtzite structure, but the superior properties of AlN along with its IC-compatibility [10] makes it the prime candidate. Another material which has attracted a lot of attention recently is $Na_xK_{1-x}NbO_3$ (NKN) owing to its extremely high piezoelectric as well as permittivity coefficients.

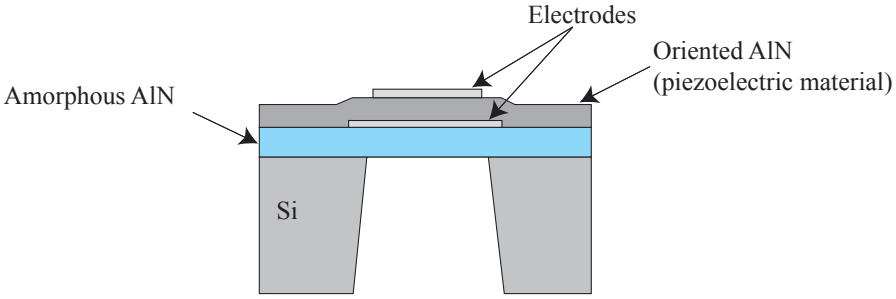

Figure 3. A membrane type BAW resonator. The membrane is released from the substrate by etching the substrate from the backside. In addition, contact holes for the bottom electrode have to be etched.

1.3 Aluminum Nitride

One very interesting material for acoustic wave applications that has gained increased popularity during recent years is AlN. Stoichiometric aluminum nitride is a very stable compound with a strong covalent/ionic bonding. The bonding energy in the structure is 11.5 eV/bond [11-15], which compared to other related materials

is relatively high. AlN is a semiconductor with a band gap of 6.2 eV [16] making it a promising candidate for future UV lasers. It is also a very good thermal conductor, with a thermal conductivity of 2 W/K/cm [17] comparable to that of pure Al, and at the same time an efficient electrical insulator. Owing to its material properties, the material is also interesting for a wide variety of other applications such as in electroacoustic devices, blue diodes, IR windows, thermal conductors, IC-passivation, decorative coatings as well as protective coatings for abrasive wear resistance. The high bonding energy is also reflected in the relatively high melting point of 2200°C [18]. Furthermore, it has very high phase velocities of 5750 m/s [19] and 11350 m/s [20] for SAW and BAW respectively, which enables fabrication of high frequency devices in the GHz region.

The piezoelectric effect, which is used in electro acoustic applications, is found in the wurtzite structured hexagonal phase of aluminum nitride, which is a noncentrosymmetric crystal in similarity with all piezoelectric materials. The layer sequence is repeated every other layer, thus the stacking sequence is ABABAB... Figure 4 shows the AlN wurtzite crystal, and the positional relation between Al and N atoms. The growth direction used in the growth of AlN for SAW and BAW applications is also indicated by the c-axis. It is difficult to generalize the crystalline form of piezoelectric materials, since the effect is found in several different crystallographic classes (cubic, hexagonal, etc.), although the lack of crystal symmetry is the common denominator (with the exception of ferroelectrics). It can be stated though, that all crystals that exhibit the piezoelectric effect also show the converse effect. That is, by applying a voltage to the material, the crystal will be strained.

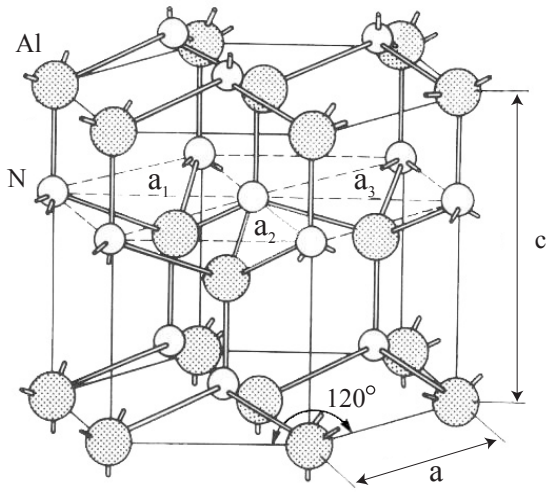

Figure 4. AlN in its wurtzite crystalline form showing the hexagonal symmetry. The direction of the c-axis is the desired growth direction in this work.

Aluminum nitride has also proven to be a very interesting electronic material in MOS technology. Since the beginning of the MOS era, SiO_2 has been the only

choice as a gate dielectric, but MOS evolution requires new materials as device dimensions are constantly shrinking. The dielectric properties of AlN, as shown in this work, puts this material in an interesting position when the next generation of gate dielectric is chosen.

Crystalline aluminum nitride can be formed in several ways such as Chemical Vapor Deposition (CVD) [21-25], Physical Vapor Deposition (PVD) [26-31], reactive evaporation, Molecular Beam Epitaxy (MBE), etc. The method used for thin film deposition in this thesis is PVD, since the focus is set on the synthesis of high quality polycrystalline AlN thin films at low temperature, which is most easily achieved by PVD deposition.

2 Film Deposition

There exist a wide variety of methods for the deposition of thin films, all having their own advantages and disadvantages. It is not the purpose of this presentation to describe all of them, nor even the most popular ones, but to describe the processes primarily used in this work.

2.1 Low Density Plasmas

A plasma can be thought of as a collection of electrons, singly and multiply charged positive and negative ions as well as neutrals and molecular fragments of different kinds. A simple and popular definition is that a plasma is a partially ionized gas which preserves its charge neutrality on the macroscopic scale. Plasma is also known as the fourth aggregation state in addition to solid, liquid, and gaseous states. It is a very energetic condition, and a favorable way to supply energy to chemical and physical processes, keeping the environment at a relatively low temperature i.e. below 100°C in most cases. The constituents of the plasma create conditions for activation of a number of chemical and physical processes which otherwise is achieved at elevated temperatures, say, hundreds and thousands degrees Kelvin.

Most plasmas, also referred to as glow discharges and widely used in thin film processing are formed by electron impact ionization of the gas in a controlled electrical gas discharge. The degree of ionization is very low, usually in the range ~10^{-5}-10^{-2}, which at normal processing pressures of 1-30 mTorr corresponds to an ion density of ~10^{9}-10^{12} cm^{-3}. This range is set by fundamental physics. A plasma density lower than the range specified above will lead to very weak electrostatic forces, thus allowing the plasma to spread over a larger volume and neutrality can no longer be maintained. Higher density is impractical to attain due to unacceptably high power densities.

Impact ionization is probably the most important process occurring in a plasma, and is in a simple form illustrated by

$$e^- + Ar \rightarrow Ar^+ + 2e^- \qquad (1)$$

There are a couple of very simple but useful relations in gas kinetics which are relevant for the discussion later and are presented here. The first formula determines the flux of particles onto a surface at a given pressure p, and is given by

$$\Gamma = \frac{p}{\sqrt{2\pi mkT}} \quad \left[m^{-2}s^{-1}\right] \qquad (2)$$

where m is the mass of the element, k is Boltzmann constant, and T is the temperature in Kelvin. The second formula relates the mean free path of a gas particle with the gas pressure. The mean free path is defined as the average distance over which a particle can travel before it collides with another particle, thus it is the distance over which the electron/ion gains energy in the presence of an electric field, and is given by

$$\lambda(mm) = \frac{p}{6.6} \quad [\text{For air, if the pressure, p, is given in Pascal}] \qquad (3)$$

2.2 Sputter Deposition

Sputter deposition is a member of the PVD family, which utilizes physical sputtering to create a source of particles (generally atoms) which subsequently condense onto the substrate and form a film. The word ”sputtering” appeared in the English language as early as 1598, and according to the dictionary it means ”To spit out in small particles with a characteristic explosive sound”. Physical sputtering is a process where atoms are ejected from a surface as a result of the bombardment of the latter by heavy energetic particles (ions). It was first discovered by Grove (1852) but did not find practical use until the beginning of the 20^{th} century.

Sputter deposition is a method used worldwide in the semiconductor industry as well as in a wide variety of other applications for the deposition of thin films onto surfaces. It is also noted that "sputter deposition" is often called "sputtering" for short by the technological community where its meaning is understood by the context, but should be distinguished from the phenomenon sputtering. Generally, sputtering offers the following advantages [32] as compared to related deposition techniques:

- Excellent film uniformity, particularly over large areas.
- Surface smoothness and thickness control.
- Deposition of films showing bulk like properties, which are predictable and stable.
- Versatility; the sputter process is essentially a kinetic process involving momentum exchange rather than chemical and/or thermal process and, therefore, virtually any material can be introduced into a gas discharge or sputtered from the solid.
- Good adhesion.
- Either conformal or planarized coatings.
- High rates, which are comparable with evaporation.

2.2.1 DC Sputtering

The simplest form of sputtering is DC sputtering, and such a system is schematically illustrated in Figure 5a. As shown in the Figure, a DC sputtering system consists of a cathode to which the target is attached, and an anode which is chamber walls usually connected to ground. The substrate can be grounded, floating, or even biased with respect to ground. Further, the system is evacuated and a particular gas at reduced pressures (tens to hundreds of mTorr) is admitted to the chamber. When a negative potential is applied to the cathode, the electric field created between the electrodes accelerates all charged particles, stochastically present in the gas in minute concentrations, and when an electron ionizes a neutral molecule according to equation (1), an electron/ion pair is created. This process continues and eventually avalanches into the creation of a plasma. At this point the

plasma will quench quickly since the ions and the electrons will eventually diffuse and be accumulated at the respective electrodes.

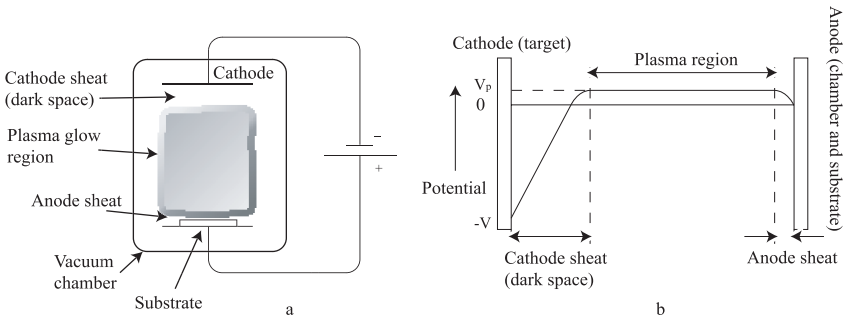

Figure 5. A typical DC sputtering system setup is shown in (a). The potential distribution of the system is shown in (b), and it is seen that the voltage drop between the plasma and the cathode is by far the greatest in the system.

Luckily, the positive ions are accelerated by the electric field towards the cathode and attain enough energy to both cause physical sputtering and equally importantly the emission of secondary electrons from the cathode surface. These secondary electrons continue the ionization process described above and are thus vital for sustaining the gas discharge. Initially the electric field is to a first order approximation constant in the space between the two electrodes, but as the plasma is excited and equilibrium conditions are established the potential distribution changes form dramatically. This distribution is visualized in Figure 5b, where the most important regions are the cathode dark space and the so-called negative glow. The latter defines roughly the boundaries of the plasma and is the region where the electric field is rather low and the electrons acquire energy, which is only sufficient to excite the gas particles, giving rise to the specific glow as a result of subsequent de-excitation. It is noted that the plasma is a quasi-neutral mixture of positive ions and negative electrons and hence is a relatively good conductor.

As a result, the electric field is predominantly confined in the space between the glow region and the cathode, also called the dark space or the sheath region. Due to the strong electric field in this region the secondary electrons are accelerated and attain enough energy at the end of their free path to cause impact ionization with a high probability. The newly created electrons continue the same process until they all leave the dark space region. The latter region is dark since initially the electron density is rather low on the one hand as well as because the excitation cross section is much lower than that for ionization at high electron energies, on the other. The thickness of the dark region scales with the mean free path of the electrons and hence inversely with the gas pressure. Perhaps, one of the most peculiar features of the potential distribution in Figure 5b is the fact that the potential of the glow region, i.e. the plasma potential is positive with respect to the anode. This is explained by the vastly different mobilities of electrons and ions due to the large difference in their masses as well as their temperatures. As a result of the different mobilities, initially the electron current onto an arbitrary surface in

contact with the plasma will be greater than the ion current. Consequently, the surface will acquire a negative potential with respect to the plasma, such that at steady state the net current onto that surface is zero (provided that the body is isolated). Thus, the plasma potential is always the highest relative to all surfaces in the chamber with which it is in contact, including the anode. The only difference at the latter is that the net current is not zero since the secondary electron current passes through it, which necessitates that the potential difference between the plasma and the anode is somewhat smaller than that between the plasma and an isolated surface. The potential of the latter with respect to ground is usually referred to as the floating potential. Both the plasma potential and the floating potential are characteristics of the plasma and depend strongly on the plasma density and electron temperature.

The gas usually used is Argon, and as noted above, the positively charged argon ions will accelerate towards the cathode and collide with its surface. The major processes occurring as a consequence of the collision are:

- The ions may be reflected, and returns to the gas phase.
- Emission of secondary electrons.
- The ions may penetrate deep under the surface and become implanted in the target material.
- The ions are likely to cause structural rearrangement in the surface layers of the target (ion induced mixing as well as diffusion).
- The ions transfer energy to atoms in the target surface, and some of them will be ejected, i.e. sputtered.

Very importantly for our purposes, the sputtered atoms leave the surface with considerable energy (several eV), diffuse through the gas phase and are eventually deposited onto the surrounding surfaces, including the substrate, thereby resulting in the deposition of a film.

2.2.2 Magnetron Sputtering

Diode sputtering suffers from several disadvantages as follows. First, the plasma density is rather low resulting in very low deposition rates. The latter is further reduced by the relatively high discharge pressures as a result of which the sputtered atoms diffuse randomly in the gas phase and hence much of the sputtered material is lost onto the surrounding surfaces. High discharge pressures mean also that the sputtered atoms are quickly thermalized through gas phase collisions and they practically land onto the substrate with thermal energies equal to that of the gas. Further, the discharge voltage is relatively high (1 to 2 kV). As a result, highly energetic neutrals (ions which are reflected off the target and subsequently neutralized) may reach the growing film and cause both a considerable damage as well as resputtering. It is noted that all these deficiencies are result of the low ionization efficiency of the secondary electrons, many of which leave the dark space with a substantial energy. This problem is to a large extent solved in the magnetron sputtering by introducing a strong magnetic field close to the target surface. Regardless of the sputter method used, a very important issue is the

generation, and concentration of electrons in the plasma. The magnetic field confines the fast electrons to the dark space by forcing them to travel along spiral trajectories due to the Lorentz force

$$F = q\left(\vec{v} \times \vec{B}\right) \tag{4}$$

Here q is the elementary charge, v is the velocity of the particle, and B is the magnetic field. As a result the electron path in the dark space increases significantly the ionization efficiency and hence the plasma density. This in turn increases the discharge current and allows the discharge voltage to be decreased down to several hundred volts.

The design of the magnetrons varies from the commonly used planar shape to cylindrical, conical, as well as rotating configurations. Another very advantageous consequence of using a magnetron, owing to the much more efficient ionization, is that the discharge can be sustained at much lower pressures, say down to 1 mTorr. Lower discharge pressures mean larger mean free path (λ), resulting in that the particles sputtered from the target retain some of their kinetic energy as they adsorb on the substrate surface. This excess energy results in increased surface diffusion, and hence film densification and in many cases improved crystal growth as discussed latter in this thesis.

One disadvantage of both pure DC and DC magnetron sputtering is the requirement that the target material has to be conducting, otherwise the target surface would eventually charge up to the applied voltage and the plasma will be extinguished.

2.2.3 RF Sputtering

A radio frequency (RF) plasma is an electrical gas discharge similar to the DC considered above, but instead of the DC power supply the discharge is driven by an RF supply, normally with a standard industrial frequency of 13.56 MHz and a peak to peak voltage of around several kV. The plasma is generated in much the same way, namely by electron impact ionization, where the electrons are accelerated by the electric field between the electrodes. It is noted that due to their high mobility the electrons follow the field within each cycle, while the ions being much heavier are hardly affected by the alternating field. This results in the formation of a substantial negative DC potential at the electrodes relative to the plasma and which potential is of the order of several hundred volts. Thus in this case, both electrodes acquire a negative DC potential and are hence both subjected to ion bombardment. It is noted, however, that this DC potential is a complex function of the current density at the electrodes. If the electrode areas are not equal then the DC potential on each of them is given by [33]

$$\left(\frac{V_{RF}}{V_G}\right) = \left(\frac{A_G}{A_{RF}}\right)^4 \tag{5}$$

Here V_{RF} is the voltage on the smaller electrode (normally the target), V_G is the voltage on the larger electrode, normally grounded, while A_{RF} and A_G are their respective areas. Since the chamber walls are also grounded then the effective area

A_G of the ground electrode is much larger than the target area and hence the DC potential at the grounded electrode is only marginal according to equation (5). The DC potential at the target according to equation (5) is much larger as shown in Figure 6. To sustain this potential difference between the two electrodes, however, a blocking capacitor is required in series with the electrodes as shown in Figure 7. In addition to the blocking capacitor a matching RF network is also used to match the output impedance of the RF generator with that of the plasma. Thus in essence the RF discharge effectively works as a DC discharge, where the cathode is at a large negative potential with respect to the plasma and is subjected to intense ion bombardment and hence sputtering.

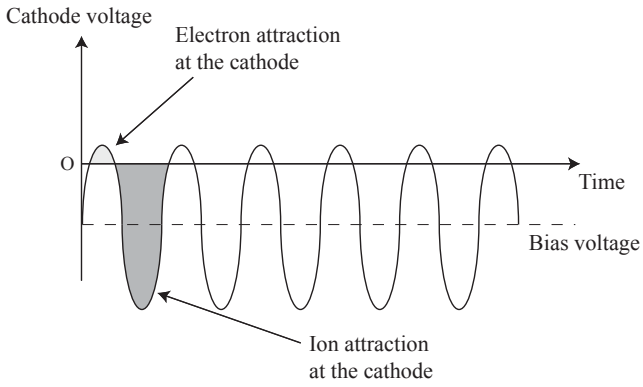

Figure 6. The cathode voltage as a function of time in an RF-system after steady state is reached. The fast electrons are attracted by the target during the positive part of the cycle. The bias voltage that develops at the target is usually several hundreds of volts.

It is noted that the plasma density in RF discharges is higher than that in DC discharges but is somewhat lower than for magnetron discharges. But by far the greatest advantage of RF sputtering is their ability to sputter dielectric materials.

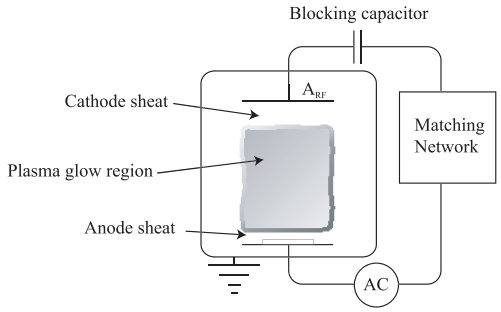

Figure 7. The figure shows an RF sputter system. To sustain the potential difference between the two electrodes, a blocking capacitor is connected in series with the latter. The substrate and the chamber wall works as the anode, whereas the target is the cathode.

Thus, any charge build up on the target surface during the negative cycle will be neutralized by electrons during the positive cycle and hence the process will continue unabated. It is also noted that the same effect can be obtained in DC sputtering by pulsing the target voltage. In other words, with a given frequency (normally several tens of kHz) a positive signal is applied to the target for a short period of time which is sufficient to discharge the target surface. This type of discharge is called pulsed DC sputtering and has become very popular for sputtering of dielectric materials due to the higher deposition rate. The latter is a serious problem in sputtering of dielectric materials, since ceramic targets must be moderately powered due to poor thermal conductivity and cracking susceptibility. In addition, their sputtering yields are normally much smaller than that of metals. The next paragraph describes a method which solves to a large extent these problems.

2.2.4 Reactive Sputtering

Reactive sputtering is a process where a metallic target is sputtered in a reactive atmosphere as illustrated in Figure 8, which for specificity shows the sputtering of Al in an Ar/N_2 ambient.

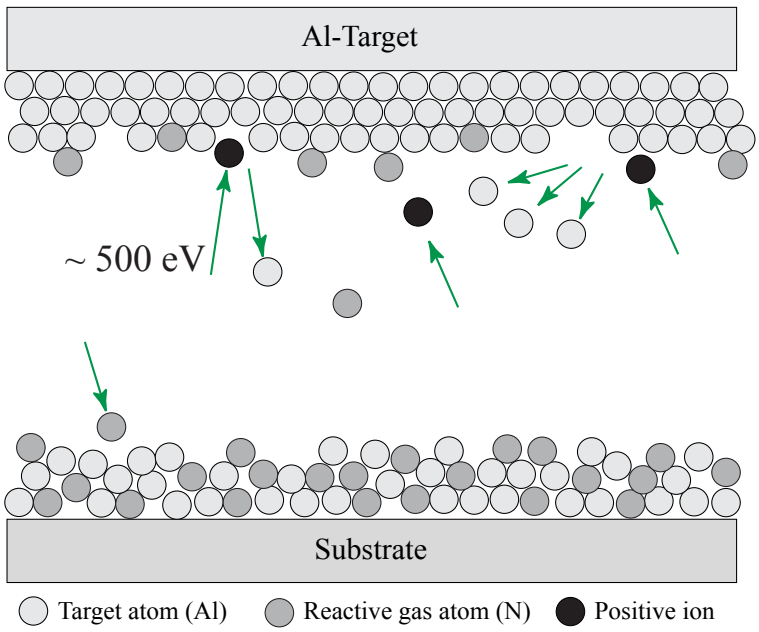

Figure 8. An illustration of the reactive sputter process, where in this case the aluminum reacts with the nitrogen to form aluminum nitride.

As the sputtered atoms are deposited onto the substrate they react with the reactive gas molecules forming thereby the desired compound. Reactive sputtering has some important advantages as compared to sputtering from a compound target:

- Metal targets can easily be machined and are cheaper.
- Metal targets have high thermal conductivity enabling efficient target cooling and hence the possibility to apply a substantially higher power, e.g. 50 W/cm^2, without melting the target.
- By employing certain tailored process techniques, high rates comparable to those of pure metals can be attained.
- A particular metal can be utilized for the synthesis of several different compounds, offering good process versatility.

There are also some disadvantages attributed to reactive sputtering. The process is extremely complex, and in order to obtain desirable results, process understanding and optimization of all the parameters influencing film quality are required. To get a better insight into the process it is instructive to take a look at its behavior as a function of the major process parameters. A typical process curve is shown in Figure 9, which shows a plot of the deposition rate vs. the flow of reactive gas, and has been divided into three different regions.

1. **Metal mode** – In this region, where the partial pressure of the reactive gas is rather low, the target is only marginally covered with compound and process behavior is almost identical to the sputtering of a pure metal target characterized primarily by high sputtering yield. As the reactive gas flow is slowly increased, however, the target surface becomes partially reacted resulting in a slight decrease in the deposition rate, since the sputtering yield of the compound is normally much lower than that of the metal.
2. **Transition region** – This is also called the hysteresis region, and is the region where a very small increase/decrease of reactive gas has a major impact on the process behavior. For simplicity of the discussion let us assume that we sputter Al in an oxygen atmosphere. As the flow of oxygen is initially increased, its partial pressure in the chamber increases accordingly, hence, the coverage of the target surface with oxide increases also, i.e. the fraction of exposed Al on the target decreases. This in turn results in a reduction of the sputtering rate and consequently in a reduction of the consumption rate of oxygen. The latter reduction results in a further increase in the partial pressure of oxygen, which in its turn causes an even larger fraction of the target surface being oxidized and so on. At this point the process avalanches uncontrollably until the whole target surface is oxidized. The net result is a substantial and steep drop in the deposition rate (see Figure 9), an equally steep jump in the oxygen partial pressure and complete oxidation of the target. Normally a decrease in the discharge voltage is also observed since the secondary electron emission coefficient for compounds is usually higher than that for pure metal surfaces. The process is now said to be in compound

mode. If at this point we start decreasing the oxygen flow then the transition to metal mode will not occur at the same oxygen flow since now the oxygen partial pressure is significantly higher than that when the target was operated in metal mode. The only way to decrease this high oxygen partial pressure is to further decrease the oxygen flow until the second transition point is reach. At this stage a small fraction of the target is metallic resulting in an increase in the sputtering yield. This in turn increases the consumption of oxygen (at the substrate) which in turn further decreases the oxygen pressure and so on. Therefore, the process avalanches uncontrollably from compound to metal mode.

The main conclusion from this simple consideration is that the deposition rate during reactive sputtering exhibits a hysteresis behavior as a function of the gas flow and secondly the transitions from metal to compound as well as from compound to metal mode are very steep. The latter observation is very important since ideally one would want to operate the process in metal mode but very near the edge of the transition region in order to deposit stoichiometric compounds. The instability of the process at this point, however, make it unsuitable for industrial applications since the slightest fluctuation would trigger the above avalanche and the sputtering process will uncontrollably and irreversibly fall into compound mode. The only way to reverse the process into metal mode is to decrease the oxygen flow substantially until metal mode operation is established and increase it carefully until the edge of the transition region is reached without overdoing it.

3. **Compound mode** – In this mode, as noted above, the target surface is completely oxidized and any further increase in the oxygen partial pressure does not affect significantly the process. The deposition rate is normally substantially reduced, and in the case of aluminum the rate drops more than one order of magnitude as the process enters the compound mode. Clearly due to the substantial reduction in deposition rate, it is in most cases desirable to avoid the process operating in compound mode, particularly in industrial applications where throughput is one of the most important issues directly related to the cost of the product.

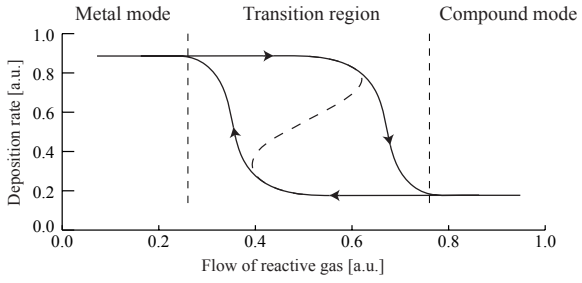

Figure 9. A typical processing curve obtained in reactive sputtering. The transition from metal mode to compound mode, as well as the other way around, is extremely abrupt.

2.2.5 Modeling of Reactive Sputtering

The complexity of reactive sputtering makes process modeling an extremely valuable tool for studying and predicting its behavior as well as developing new technical solutions. Westwood [34] showed a way to describe the hysteresis behavior, although the most detailed theoretical model has been developed by *Berg et. al*. [35-44]. The latter basically erects balance equations at steady state for the gas flow and gas consumption at the various surfaces as well as the of the sputtered fluxes. The model has also been applied in several PhD thesis [45, 46], where modified versions have been developed for specific applications. The best general description of the model can be found the doctorial thesis by Dr. Nyberg and in *Handbook of Thin Film Process technology* [46, 47], which also presents a detailed discussion and justification of the assumptions and simplifications made in the model.

The model can in its initial form predict the sputter rate, composition of the deposited film, partial pressure of the reactive gas, the width and the position of the hysteresis region as well as the fraction of the target which is covered by compound. In addition, the model can be modified to enable modeling of complex configurations of the reactive sputter process like e.g. co-sputtering from two targets, and reactive sputtering employing the "baffled target" setup, as demonstrated later in this thesis.

2.3 Thin Film Growth

Materials can be divided into three different categories, single crystalline (SC), polycrystalline and amorphous respectively, depending on the short and long range ordering of the atoms in the lattice. In the SC case, all the atoms are perfectly ordered in a regular and periodic lattice. This ordering results in that each crystal possesses a specific symmetry. The smallest cell which still preserves this symmetry is called a unit cell. The edges of the latter coincide with the axis of symmetry and their lengths define the so-called lattice parameters. In contrast, amorphous materials have no apparent ordering and hence their structure does not have any symmetry. One can think of amorphous materials as having a random but uniform structure, which in addition satisfies a stoichiometry requirement even on the atomic level. Due to this randomness of the structure amorphous materials look identical in all directions and hence all material properties are isotropic. Polycrystalline materials consist small crystals also called crystallites or grains. The periodicity of the lattice is broken at the boundary between two crystallites, or the boundary may be amorphous or even be hollow (so called voids). In short, the crystallites have generally different orientation relative a common coordinate system. The dimensions of the crystallites may vary from several nanometers to tens of micrometers or more. Thus, polycrystalline films are primarily characterized by the size of the crystallites (grain size), their relative orientation (texture) and density. In many applications it is advantageous if the crystallites have a predominant orientation, i.e. most of them (if not all) have one and the same axis of symmetry oriented in a specific direction. Such films are called highly textured (or highly oriented).

A critical issue during film growth is the deposition temperature. It is almost unavoidable that a film is deposited at one temperature, whereas the component it is part of is used in a completely different temperature interval. Thus, the difference in thermal expansion between the film and the substrate material is very likely to be a source of stress in the film, which in the worst case may lead to severe adhesion problems or even destruction of the film. Nevertheless, the difference in thermal expansion is not the only problem encountered during thin film growth. Thin film growth is also very dependent on the surface cleanliness, energy available at the surface, and the substrate lattice where nucleation takes place. Growing e.g. Si on Si, where the lattices of the film and the substrate match perfectly is called homoepitaxy. However, during deposition of III-V semiconductors like AlN onto SiC, GaAs, or sapphire, there is a slight crystallographic mismatch between the film and the substrate, thus the film stretches or contracts in order to better "fit" and accommodate this mismatch. Such crystal growth processes are called heteroepitaxy. If the mismatch is rather large then epitaxial growth is impossible and the film grows as polycrystalline at best.

During sputtering, particles sputtered from the target travel through the plasma, and eventually end up on the substrate. Several different mechanisms are responsible for how the species actually attach to the surface, and take active part in the film formation. The energy available at the substrate surface, either in the form of elevated temperatures or provided by particle bombardment, etc., strongly affects crystallization of the film. Figure 10 illustrates a possible film growth mechanism for processes with high (high-T) and low (low-T) atom mobility respectively. The figure illustrates also how the ad-atoms move about on the surface through a process called surface diffusion in order to find a low energy position.

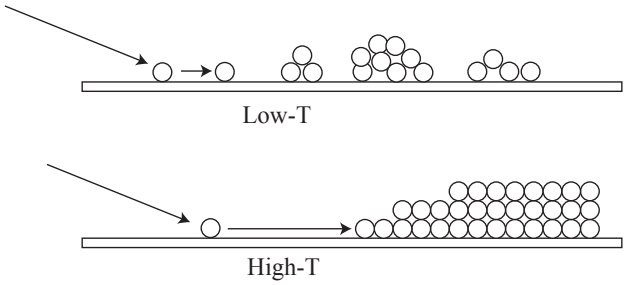

Figure 10. The figure shows the difference in surface mobility at different temperatures. At high T, the adsorbed atom diffuses on the surface to find a low energy position, which promotes crystalline growth.

Thornton et. al. [48, 49] have developed an empirical model based on the relation between the structural growth and the material's melting point. The model states that T/T_m, where T_m is the melting temperature of the material, determines the structure of the growing film. At $T/T_m < 0.1$, the adatom surface mobility is poor, and the film seems to grow in the direction of the material flux. The result is an under dense film rich of voids, with a pebble like structure, although individual crystallites may have near bulk density. In the region $0.1 < T/T_m < 0.3$ adatom

surface diffusion is initiated, and the film reaches a density closer to bulk values. Grain boundaries rather than voids are separating the grains. At $0.3 < T/T_m < 1$, surface mobility is considerable, and columnar growth is not unusual. Even grains extending trough the entire film are possible, which lowers the fraction of voids and grain boundaries.

This simplified model gives an apprehension about the resulting film quality with respect to the melting point of the material to be deposited. Nevertheless, as mentioned before, there are of course other factors that also influence the resulting film structure in plasma assisted deposition processes, such as ion energy, process pressure, target-to-substrate distance, etc.

3 Etching

Etching is a term, which denotes partial or complete removal (erosion) of materials. Etching can be effected through a variety of mechanisms, ranging from chemical, physical, or a combination between the two. Depending on the phase of the etching agent, etching is formally divided into two categories, dry and wet respectively. Dry etching refers to processes where the reactive species are either in a gaseous form and/or as energetic ions normally generated by a plasma discharge, while wet etching refers to processes where the etching medium is in liquid form. The two most important characteristics of the etching process are the etch rate of a particular material as well as its selectivity with respect to other materials, i.e. the ratio between the etch rates of two specific materials. In the early seventies, when the Critical Dimension (CD) in microelectronic fabrication was in the order of several micrometers or more, i.e. much larger than the film thickness, wet chemical etching was commonly employed owing to its high etch rates and extremely high selectivity. In modern IC-fabrication, however, the CD is comparable or much smaller than the film thickness which imposes stringent requirements on the etch process, and particularly on its anisotropy (directionality). For exact pattern delineation, dry etching processes have been steadily developed which exhibit excellent anisotropy. Figure 11 illustrates schematically the basic difference between wet and dry etching.

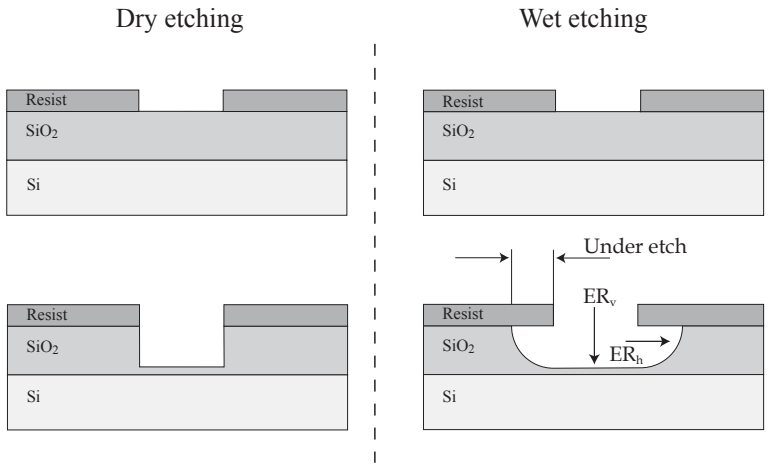

Figure 11. The difference between a dry etched and wet etched structure is shown. As seen in the figure, decreasing dimensions require the anisotropy found in dry etching techniques for pattern delineation.

In the first instance the loss of CD is substantial when the film thickness is comparable or larger than CD, while in the second instance we have an exact pattern transfer from mask to film. Another important characteristic of dry etching is that it is generally insensitive to the film texture, i.e. crystallographic orientation of the film, and hence films with different textures have similar etch rates. Modern

dry etching processes often employ a combination between dry chemical and physical sputtering. Thus for instance a plasma is an excellent source of highly reactive radicals and excited atoms/molecules and at the same time a source of energetic ions which bombard the film to be etched, thus enhancing and promoting chemical reactions at the surface. The development of highly sophisticated and specialized etch processes together with the development of equally sophisticated photolithographic processes have been the main driving force behind the sustained development of the semiconductor industry according to the Moore's law. The rest of this section will be devoted to dry etching.

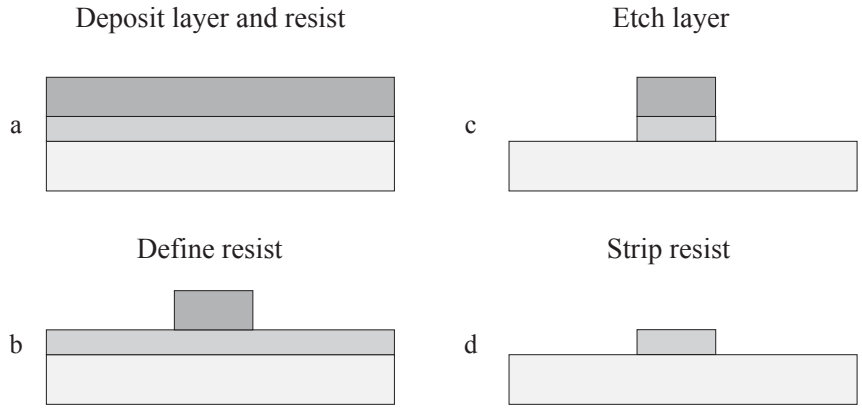

Figure 12. The figure shows a typical dry etching mask step. The complete structure with photoresist (a) is exposed and developed (b). The dry etch removes the material not covered by the resist (c), and after resist removal the resist pattern is transferred to the thin film.

A typical dry etching step in thin film processing is schematically shown in Figure 12. In reality, however, the etch profile may not be as perfect and a certain lateral etch may occur resulting in mask undercut. The process anisotropy, A, is a measure of the undercutting, and is the ratio between the vertical etch rate ER_v and the horizontal ER_h etch rate

$$A = 1 - \frac{ER_h}{ER_v} \tag{6a}$$

The selectivity of the etch, as noted above, is another important characteristic of the etch process. The selectivity S_{ab} is the ratio of etch rates between the layer to be etched ER_a and the resist or the layer to be etched and the underlying layer ER_b. This is expressed as

$$S_{ab} = \frac{ER_a}{ER_b} \tag{6b}$$

$$U = \frac{ER_{middle} - ER_{edge}}{ER_{middle}} \tag{6c}$$

A third important property is the uniformity, U, which is a measure of the etch rate variation over the whole wafer. Finally, the etch rate is primarily increased by the generation of high density plasmas as discussed in the next paragraph.

3.1 Etching Plasmas

There exist a variety of ways to generate a plasma for dry etching applications. DC is replaced by various RF sources due to the more efficient plasma generation and the possibility to maintain a gas discharge independently of the cathode conductivity. Also the choice of gas has a great impact on the process. It should preferably be nontoxic and stable for storing and transport purposes, while at the same time produce highly reactive species upon decomposition as well as volatile species upon reaction with the material to be etched.

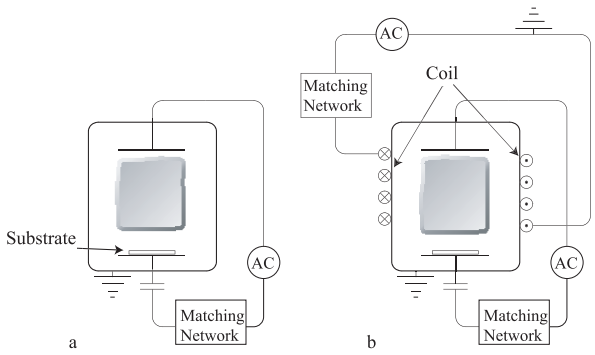

Figure 13. The difference in system configuration for a RIE (a) and an ICP (b) etching system. The coil in this case is wired around the chamber, although it is also possible to place the coil in the lid.

The simplest dry etching configuration is called reactive ion etching (RIE), in which the generation of reactive species and the bias that builds up on the substrate are created by one and the same electrical circuit, as shown in Figure 13a. This results in that both the plasma density and the bias voltage increase simultaneously as the discharge power is increased. However, when processing small structures, and more importantly, when etching materials sensitive to ion bombardment it is desirable to control the plasma density independently of the bias voltage. This is achieved by employing two independent power supplies, one for the plasma generation and another for supplying bias to the substrate holder. In modern IC-fabrication the so-called inductively coupled plasma (ICP) reactors are generally used. In an ICP system the power from the RF source is inductively delivered to the plasma, while the substrate bias is independently provided and controlled by an ordinary RF capacitive discharge. The plasma density in these systems is by almost an order of magnitude higher than that for RIE systems resulting in high etch rates. In addition, the high ionization efficiency of ICP discharges allows operation at reduced pressures resulting in an improved process anisotropy. A typical ICP system is schematically showed in Figure 13b.

3.2 Etching Mechanisms

The major erosion mechanisms in dry etching are physical sputtering, chemical etching, and often synergistic combinations between the two as illustrated in Figure 14. Physical sputtering is characterized by excellent anisotropy (see Figure 14a) due to the directionality of the ion flux, low sputtering rates, poor selectivity, and it introduces structural damage as well as suffers from secondary processes, such as ion reflection and redeposition of the sputtered material. That is why physical sputtering is used in special cases only. Chemical etching, on the other hand, exhibits high etch rates, excellent selectivity but suffers from very poor anisotropy (see Figure 14b). Clearly, the two types of erosion processes complement each other very well and by making a suitable combination between the two results in a dry etching process which exhibits excellent characteristics (see Figure 14d) - high etch rate, high selectivity, high anisotropy and produces low residual damage. That is why modern dry etch processes almost exclusively utilize chemical etching in combination with ion bombardment. In order to get a better insight we look at the most important steps in a dry etching process, which determine to a large extent the behavior of the process. These are:

1. Generation of reactive species such as ions, excited molecules, and particularly highly reactive radicals.
2. Transport of reactive species as well as ions through the plasma to the substrate surface.
3. Adsorption, preferably chemisorption, at the substrate surface. Species that attach to the surface through physisorption are likely to either desorb from the surface or become chemisorbed.
4. Diffusion of reactive species on the substrate surface.
5. Now the chemisorbed species react with atoms in the film, and form by-products that initially stay chemisorbed on the surface.
6. Desorption of volatile by-products from the substrate surface.
7. Transport of the desorbed by-products to the gas phase (plasma), and their subsequent removal by the pumping system.

One of the greatest advantages of using ion bombardment in a dry etching process is the possibility to control many of the above steps and particularly to stimulate chemical reactions, desorption of reacted species, surface diffusion, prevent surface passivation, etc. A typical approach to achieve extremely high anisotropies is to add small quantities of a gas that does not form volatile compounds with the material to be etched. Thus, areas which are not exposed to ion bombardment (normally side walls or areas under the mask) are passivated, which results in blocking of the reaction. The passivating layer on areas exposed to the ion bombardment, however, is constantly sputtered by the latter and hence the etch process proceeds exclusively in the direction of the ion bombardment, resulting in a perfect anisotropy (see Figure 14c).

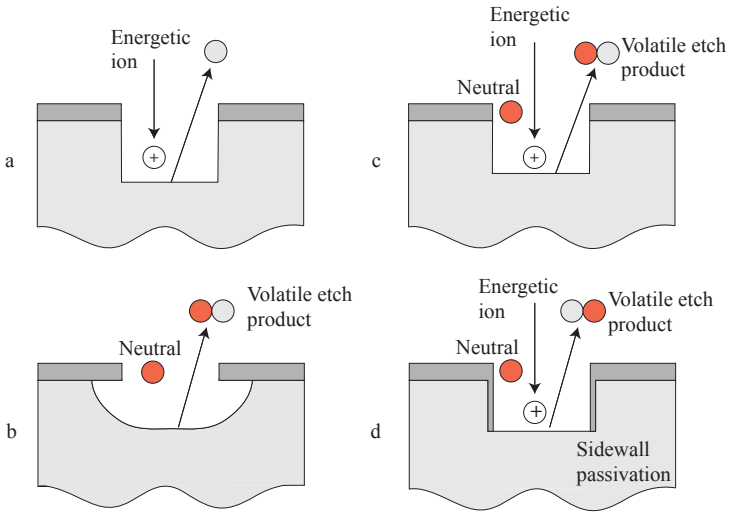

Figure 14. The figure illustrates the different etch mechanisms in dry etching, which are (a) physical sputtering, (b) chemical etching, (c) ion assisted etching, and (d) inhibitor etching.

Further, combining ion bombardment with chemical etching results often in substantial synergism. This type of processes are normally referred to as ion assisted etching and was first demonstrated by Winters and Coburn [50] in a very famous experiment in the late seventies. In this experiment, poly Si was dry etched in a XeF_2 atmosphere (note that this gas etches Si spontaneously), and by Ar ion bombardment.

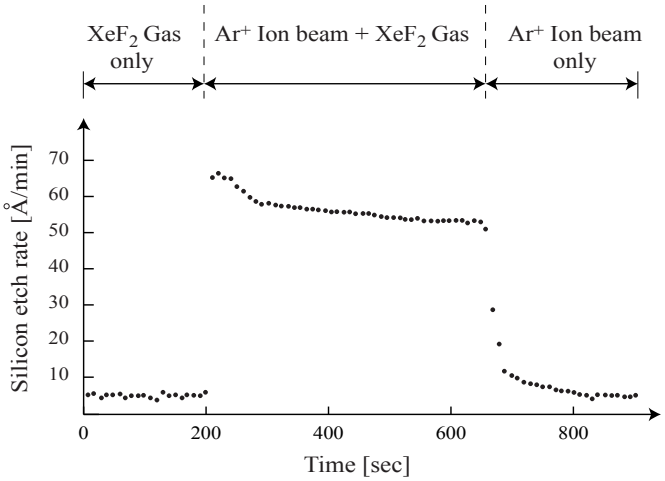

Figure 15. The figure shows the result from the famous ion assisted etching experiment performed by Winters and Coburn [50].

As shown in Figure 15, neither the fluorine gas nor the ion bombardment alone result in high etch rates. Thus, the etch rate in the first case was about 5 Å/min, and in the second even lower. However, when the silicon was exposed to both the gas and the ion bombardment simultaneously, the etch rate increased dramatically and reached a value of approximately 60 Å/min, i.e. an increase of more than a factor of ten. The explanation for the significant increase in etch rate is that as the ions impinge the substrate surface, energy is transferred to the atoms in the top layer, facilitating breaking of bonds and surface diffusion. Hence, the formation of volatile species on the surface as well as their subsequent desorption is greatly enhanced, resulting in substantially higher etch rates. It is this synergism as well as the resulting anisotropy which has made ion assisted etching as the main method for pattern delineation in IC-fabrication. In recent years etching processes producing structures with practically infinite aspect ratios have been developed. One such example is the deep etching of Si, which is a complex two step process of wall passivation and etching. There exist two major recipes, the cryo etching and the Bosch process respectively. The latter is briefly described since it is used in some of the work in this thesis. The Bosch process is based on three steps, which are cyclically repeated until the desired depth is achieved. In the first step, all surfaces are covered with a polymeric film. In the second step, the latter is removed from horizontal surfaces by directional ion bombardment. In the last step Si is chemically etched with a very high rate, which also results in the complete removal of the passivating layer on the sidewalls, which necessitates repetition of all three steps. The following is basically one cycle in the Bosch process:

1. The chamber is filled with C_4F_8 that polymerizes all surfaces in the system. No bias is used.
2. The chamber is now filled with argon and SF_6, and the bias applied efficiently removes the passivating layer on all horizontal surfaces.
3. Even more SF_6 is added, and the fluorine reacts with free silicon exposed to the plasma.

All steps in the process are rather short, thus the matching network has to be particularly fast to keep up with the change of plasma conductivity as a function of different gas mixtures. One also realizes that evacuation of the gas in the preceding step can never be total, thus the process will never reach equilibrium. That means it is an engineering problem rather than a theoretical issue to optimize the process.

4 Material and Device Characterization

This section will briefly describe the different analytical methods used in this thesis for material and device characterization.

4.1 X-ray Diffraction

X-ray diffraction is a very important analytical technique used to extract information about materials having some degree of crystallinity. Each crystalline solid has its own characteristic x-ray powder pattern, and by determining the "fingerprint" of the material, identification is possible. This of course requires a sample in the form of a powder, thus sample preparation methods like milling is necessary. However, x-ray diffraction does not have to be destructive. When analyzing samples where the phase is already known, determination of film quality can be done by relative comparison of one single reflection in the sample. Thus, entire wafers can be inserted in the instrument, and further processed after examination if necessary. The technique can be used to ascertain the crystal structure, lattice constant, lateral displacement, grain size, defect density etc. in both the substrate and the deposited film as well as the relation between them. The data can be further used to deduce e.g. stress and strain induced into the film during film growth.

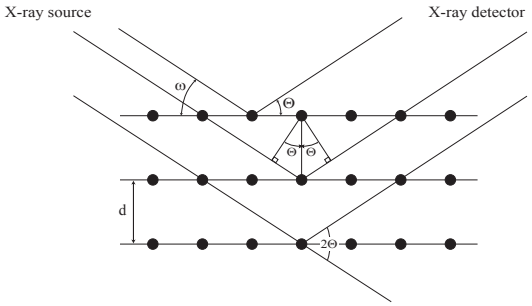

Figure 16. The figure illustrates the XRD setup. When the condition for Bragg's law is satisfied it results in constructive interference.

The method is based on the Bragg reflection as described by equation (7), where Θ is the angle of incidence, d is the spacing between planes in the crystal structure and λ is the wavelength of the x-ray source, usually copper with λ = 1.54 Å. When the Bragg condition is satisfied, that is, the distance traveled through the

$$2d\sin\theta = n\lambda \qquad n = 1, 2, 3, ... \tag{7}$$

material is equal an integer times the wavelength, the diffracted rays are in phase and interfere constructively as illustrated in Figure 16. It is important to point out that at angles other than the Bragg angle, the reflected rays will interfere destructively, thus canceling out each other.

θ-2θ Scan

The x-ray source and the x-ray detector are coupled during the scan such that the incident angle and the reflected angle equal each other, that is, $\theta = \omega$ in Figure 16. The 2θ angle is swept in an interval defined by the user to find the specific angles at which the Bragg condition is fulfilled. This will occur only at planes parallel to the substrate surface.

Rocking Curve

The x-ray source and detector is fixed at a specified 2θ angle. The substrate is then moved back and fourth (rocked), which means that $\theta \neq \omega$, making it possible to perfectly align the diffracting planes and the x-ray path. The method is used to determine small changes in the lattice parameters caused by either induced stress or grain size effects in the deposited film. In addition, the full width half maximum (FWHM) of the rocking curve peak is a good measure of the orientational quality of the film.

4.2 Rutherford Back Scattering - RBS

This technique is based on elastic atomic collision (Coulomb interaction between nuclei) between fast ions and film constituents. The analytical beam consists of mono energetic light ions, normally helium or hydrogen with energies between 1 and 2 MeV. As a result of binary collisions a significant fraction of the incident beam will be backscattered. By analyzing the energy of the backscattered ions, given the analytical geometry, it is straightforward to determine the atomic mass of the analyzed film. Thus, the backscattered particles are detected by an energy dispersive detector, set only to detect ions scattered at a fixed angle. The energy loss has two major components:

- The ions lose energy (so called electronic or inelastic losses) while traveling through the sample, both before and after the collision. Typical inelastic losses for an incident 2 MeV He^+ is between 100-800 eV/nm.

- The ions lose energy in the collision with an atom. This energy is dependent on the masses of the incident nuclei and the target atoms, and is governed by a Coulomb interaction. The lighter the target atoms are, the greater is the energy separation between backscattered particles.

As the mass of the target atoms increases, momentum transfer will decrease, resulting in a reduction of the mass resolution. Therefore, mass resolution is significantly better for light elements, whereas for heavy elements, resolution is rather poor. Well worth noting is that small amounts of a light element in a heavy matrix are very hard to detect, at least with acceptable accuracy due to spectrum overlapping.

4.3 Electron Spectroscopy for Chemical Analysis – ESCA

This technique is based on the photoelectric effect, which postulates that a material exposed to x-ray radiation (usually Mg or Al K_α x-rays), ejects photoelectrons. The electrons are collected in an energy dispersive detector, and the energy measured equals the kinetic energy of the incident photon after subtracting the binding energy of the electron to its orbital. However, a small correction has to be made in order to account for the work function, which is the energy required for the electron to leave the sample surface. Thus, ESCA is an extremely surface sensitive method, due to the short range of the photoelectrons that are emitted from the solid. Nevertheless, bulk properties can still be investigated, since most ESCAs are equipped with an ion gun, enabling sputtering to the desired depth.

The greatest advantage using ESCA is the possibility to identify chemical shifts in the spectrum arising from the energy differences due to chemical bonding. For instance, an electron ejected from aluminum bonded to oxygen, exhibits an energy different from an electron ejected from aluminum bonded to nitrogen. Another advantage of using ESCA over other similar methods (e.g. Auger Electron Spectroscopy) is that the sample is irradiated with x-rays, as compared to electrons that are much more likely to damage the surface when doing in-situ measurements during film growth. ESCA is normally used for compositional and chemical analysis. The resolution of the method is about 0.5 atomic-%.

4.4 Atomic Force Microscopy – AFM

An atomically sharp tip is scanned over the surface to be investigated, and by detecting the vertical movement using a laser, the surface can be replicated. The sharp tip is assembled at the end of a soft cantilever spring.

There is also another mode of AFM, based on the forces between the atoms in the tip and the atoms in the sample as a function of distance between them. When the tip and specimen are widely separated, the van der Waals force pulls them together, whereas for smaller distances the orbital overlap, hence the tip and the specimen surface are kept apart by electrostatic repulsive forces.

AFM is a very powerful technique in materials science, since morphological information on the nanometer scale can be obtained relatively fast, due to the fact that this type of microscope does not require operation under vacuum.

4.5 Electrical Characterization

Measurement of the electrical as well as the electroacoustic properties of the materials has been done using the instruments listed below. Electro acoustic measurements have mostly been done on FBAR's or transversal SAW's. Dielectric, as well as leakage current measurements where done using MIM and MIS structures.

HP 4280A CV Meter **–** The capacitance and the conductance of the test structure is measured as a function of applied voltage at 1 MHz. A needle like sharp probe is used to electrically contact the sample, and the probe station is enclosed in a metal box for electromagnetic isolation.

HP 4156 IV Parameter Analyzer – The current is measured as a function of applied voltage at DC conditions. The same probe station as in the CV setup is used.

HP 8720D Network Vector Analyzer – The network analyzer does not have any reference plane of its own, thus accurate calibration is mandatory to achieve reliable results. Calibration was done employing Impedance Standard Substrate from Cascade Microtech using an open-short-load and transmission-reflection-load configuration for one port and two port measurements respectively. The probe used to contact the sample was a Coplanar RF probe with a 150 μm pitch. The instrument measures S-parameters, in a one port or a two port configuration in the range 50MHz – 20 GHz. The S-parameters are S11, S12, S21, and S22, although in a symmetric device only two of them are relevant. S11 and S22 are defined as the electrical energy reflected back to the generator compared to the electrical power given by the generator, whereas S21 and S12 are measures of the electrical power transmitted through the device under test (DUT).

5 SAW and BAW Devices

As noted in the introduction, the main focus of this work is to develop synthesis processes of highly oriented AlN thin films in view of electroacoustic applications. Thus, characterization of the electroacoustic properties of the films is essential for their final evaluation. It is noted that the properties of interest here are the SAW and BAW electromechanical coupling (K^2 and k_t^2 respectively), SAW/BAW velocity, Q-factor, propagation losses, temperature coefficient of delay, etc. These quantities are sensitive functions of the film properties (texture, orientation, density, surface roughness, etc.) as well as those of the substrate. Thus for instance, the coupling coefficient depends strongly on the film texture, i.e. the smaller the FWHM of the rocking curve (for a particular preferred orientation, say, c-axis in this work) the higher the electromechanical coefficient is. Further, this condition is necessary but not sufficient. Since the c-axis of AlN is directional it is important that the majority of the crystallites are unidirectionally oriented, otherwise the piezoelectric contributions from antiparallel grains will mutually cancel out, resulting in a material which is piezoelectrically dead. The Q-factor depends strongly on the quality of the film, particularly its density, and defect concentration. Equally so do the propagation losses depend on film density and surface roughness. Impurity concentrations also decrease the quality of the film and affect in a similar way its electroacoustic properties. This section presents basic methods and tools for electroacoustic characterization of piezoelectric materials and particularly thin films for both SAW and BAW applications.

5.1 SAW Devices

The electromechanical coupling K^2 (as well as k_t^2 for that matter) is a measure of the efficiency with which electromagnetic energy is converted to mechanical. It is a direct function of the piezoelectric tensor and hence of the orientation of the film. A popular approximation for K^2 is given by

$$K^2 = 2\frac{v_s - v_a}{v_s} \tag{8}$$

where v_s is the stiffened SAW velocity and v_a is the unstiffened SAW velocity. The former is derived from the center frequency, while the latter is experimentally measured by short circuiting the surface along the propagation path by depositing a thin conductive layer. Another method for determining the coupling, among other parameters, is by computer modeling. There exist a large number of models, some more approximate, others more accurate but at the same time more time consuming. One of the most popular models, which provides good balance between accuracy and speed, is the so called COM model [51-55]. The latter utilizes the impedance response of a SAW resonator to extract the main electroacoustic parameters or alternatively the latter can be modeled from given material constants and geometry. It is noted that the coupling for SAW modes is

normally much lower than that for BAW modes. This is particularly important for bandpass filters, where the bandwidth is equal to the electromechanical coupling.

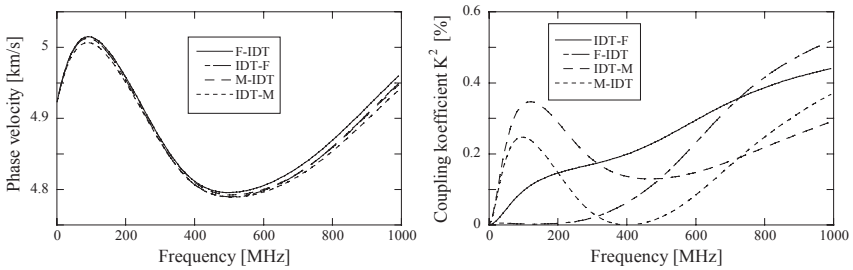

Figure 17. A computer program, LAYERS, has been used to obtain the dispersion curves for the coupling coefficient as well as the phase velocity for different IDT configurations.

Another useful model [56] describes SAW propagation in layered materials which particularly important for thin film SAW devices. Thus, it follows that both the electromechanical coupling as well as the phase velocity are dispersive functions of frequency. A computer program called LAYERS has been used to calculate these dispersion curves for the specific combination used. By way of example, Figure 17 shows the frequency dependence of the SAW velocity and the coupling coefficient for a thin film structure consisting of 2.1 μm AlN, 0.7 μm SiO_2 deposited on (100) silicon. In addition, there are four different configurations (shown in Figure 18) depending on the location of the Inter-Digital Transducers (IDT) and an optional short circuiting plane as follows.

- Case 1: IDT-F means that the IDT's are located on top of the piezoelectric film without a short circuiting plane
- Case 2: F-IDT means that the IDT's are located under the piezoelectric film without a short circuiting plane
- Case 3: IDT-M means that the IDT's are located on top of the piezoelectric film with a short circuiting plane under the latter
- Case 4: M-IDT means that the IDT's are located under the piezoelectric film with a short circuiting plane on top of the latter

The wave propagation is in the [110] direction of the Si substrate. There are three main factors which one wants to derive from the above curves, namely the coupling coefficient, the operating frequency and the phase velocity, and clearly, both the coupling and the phase velocity are complex functions of frequency. In choosing these three parameters it is advantageous that the phase velocity has a zero derivative at the operating frequency if one wishes to minimize the group delay time. On the other hand, one would also want to have as high coupling as possible, so that the final choice is determined by the type of application. In our case we have chosen to work at frequency of around 500 MHz where the phase velocity has a zero derivative, while the coupling coefficient for the case IDT-F is in the range 0.2-0.3%. The propagation losses can be estimated directly by

measuring the attenuation along the propagation path. This method has also been employed in this thesis.

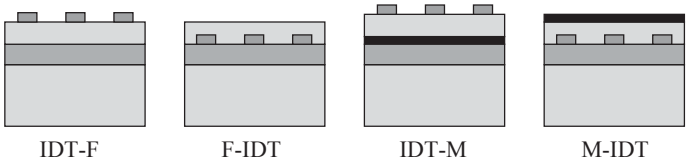

Figure 18. Different IDT configurations that has been simulated in LAYERS.

5.2 BAW Devices

Similarly to the SAW case the electroacoustic properties of a BAW device are sensitive functions of the film quality and orientation. A typical building block in BAW devices is a BAW resonator. It consists of an acoustic cavity (normally a piezoelectric material) which is bounded on both sides by metal electrodes. This sandwich structure is usually acoustically isolated from the supporting substrate, either by creating a gap between the bottom electrode and the substrate which was shown in Figure 3, (so called membrane resonators) or by fabricating a Bragg reflector (so called solidly mounted resonators) - see Figure 19.

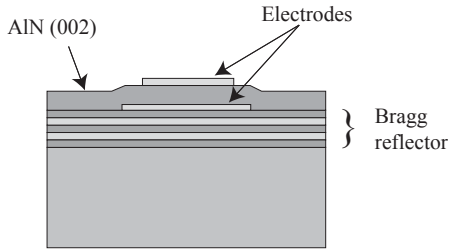

Figure 19. The figure shows a Bragg resonator. The reflector itself is a sandwich structure of acoustically high impedance and low impedance layers.

The impedance characteristic of such a resonator are readily modeled by solving the equations of motion coupled with Maxwell's equations and taking into account the finite geometry [57]. One such popular model is the Nowotny Benes model [58, 59] which also takes into account both the losses and the acoustic propagation in the electrodes. Given the materials constants and the geometry of the resonator one easily find the impedance response as illustrated in Figure 20.

The resonator simulated in Figure 20 consists of 2 μm thick c-axis oriented AlN film and 300 nm thick Al electrodes on either side. As seen, the impedance response is mostly capacitive apart from the resonance region where the impedance is inductive. Resonators are most useful in their inductive regions. The frequency separation between the two points where the impedance becomes real is in fact a measure of the electromechanical coupling

$$k_t = \frac{\pi}{2}\sqrt{\frac{f_a - f_r}{f_a}} \tag{9}$$

The same is true for an experimentally measured resonator response, provided that the parasitic capacitances and inductances have been accounted for. Similarly, the resonator Q-values is calculated from

$$Q = \frac{f_r}{\Delta f_r\big|_{-3dB}} \tag{10}$$

where the frequency separation is measured at constant conductance. It is readily shown that if the losses in the electrodes are negligible then the quality factor of the resonator is equal to that of the material [60].

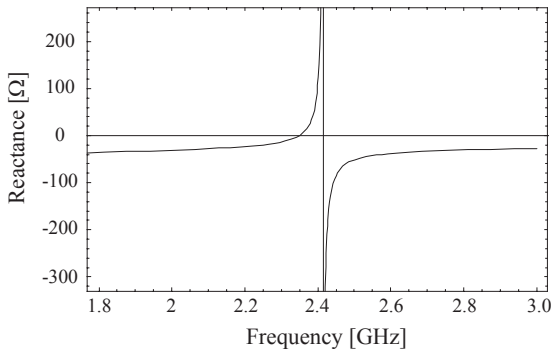

Figure 20. Reactance for a Bragg resonator as generated by the Nowotny-Benes model for a 2 μm AlN film surrounded by 300 nm aluminum electrodes.

5.3 Fabrication of SAW and BAW devices

This paragraph serves to describe briefly the main steps used in this work for the fabrication of BAW and SAW devices as well as outline the differences between them. All patterning steps are performed using standard lithography processes, with a positive photoresist and a commercially available developer.

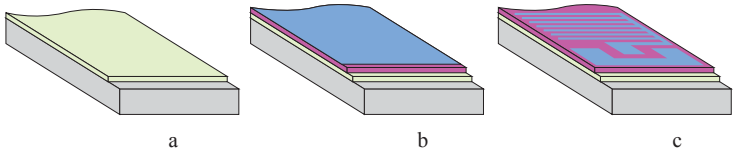

Figure 21. Schematic of the fabrication steps of a SAW.

The fabrication sequence of a SAW IDT on Si substrates is illustrated in Figure 21, and includes the following main steps:

- Commercial 4" singly polished Si wafers with a resistivity between 3 to 7 kΩcm are cleaned using a standard cleaning procedure. The use of highly resistive Si wafers is needed to eliminate the parasitic capacitance through the substrate.
- The wafers are then thermally oxidized in a furnace at 1050°C and a SiO_2 layer of a desired thickness is grown as shown in Figure 21a.
- A highly (002)-oriented polycrystalline AlN film is deposited on top of the SiO_2.
- An Al layer is then deposited over the AlN layer as shown in Figure 21b.
- The aluminum is finally patterned, and the resulting IDT pattern is shown in Figure 21c.

As seen from the above description, fabrication of SAW devices is not very complicated. The two most critical steps are the deposition of the AlN film as well as the patterning of the electrodes. The performance of a SAW device is rather sensitive on the shape and the geometry of the electrodes. In particular, the metallization ratio (defined as the ratio between the electrode width and that of the gap between two neighboring electrodes), the metal thickness, and the sidewall profile are three very important parameters. That is why patterning of Al over AlN has been studied in great detail in this work. It is noted that Al is de facto the standard electrode material for SAW applications because it is light, and hence introduces minimal perturbations due to mass loading as well as has very low resistivity - two excellent properties unrivaled by any other metal. In addition, Al has a high Q-value, which is particularly important for BAW devices. The above sequence is also used for the fabrication of SAW devices on substrates other than Si.

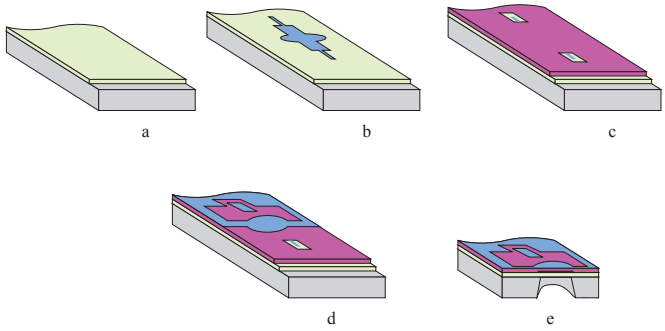

Figure 22. Schematic of the fabrication steps of an FBAR.

The fabrication of BAW resonators follows a somewhat different scheme. The following is a typical fabrication sequence for the fabrication of a BAW resonator of membrane type.

- Commercial 4" singly polished Si wafers with a resistivity between 3 to 7 kΩcm are cleaned using a standard cleaning procedure
- An amorphous AlN film is deposited (see Figure 22a), which will function as a supporting layer as well as an etch stop later on in the processing scheme when the structure is etched from the backside.
- The bottom electrode, in this case Mo, is deposited and patterned, which is shown in Figure 22b. The reason for using Mo instead of Al is explained later.
- A highly (002)-oriented AlN film is then grown. The AlN is patterned by dry etching to open contact holes down to the Mo bottom electrode as illustrated in Figure 22c. The use of Mo instead of Al is of great importance in this step. Since selectivity of the etch process between AlN and Al is rather low, then the use of Al as bottom electrode would result in poor control of the end point in this etch step. An eventual overetch would result in increased serial resistivity, while incomplete etch would result in a poor electrical contact. For this reason Mo is used as bottom electrode due to high process selectivity. In addition Mo has good conductivity as well as has a high material Q-value.
- An Al layer is then deposited for the subsequent formation of the top electrode. The Al is patterned using dry etching (see Figure 22d). Here, Al is etched on top of AlN, thus the great selectivity between the Al/AlN is required - an issue which has been addressed in this work as described below.
- Finally, the Si is dry etched from the backside of the wafer, to create a freestanding membrane – an FBAR. This is also a very critical step, since the membrane after removal of the underlying silicon is only a few μm's thick. Fortunately, the selectivity between Si and amorphous AlN is extremely high and this step is performed with relative ease. A cross section of the final structure is shown in Figure 22e.

As seen from the above sequence the fabrication of BAW devices is relatively more complicated which stems from the necessity of defining a bottom electrode as well as creating acoustic isolation from the substrate. High etch selectivities are required in all four etch steps. On the other hand sidewall control is not essential due to the relatively large dimensions of the resonator, which is of the order 0.1 mm^2 for a resonator operating at a frequency of 2 GHz.

6 Results

In this chapter, the major results obtained in this thesis are summarized. Most of the results can also be found in the Papers I-IX, but there are also results included here that have not been published yet. The results in this chapter will be presented in the same order as they appear in the fabrication sequence of SAW/BAW devices. Finally, in chapter 7, a very short summary of Paper I-IX will be given.

6.1 Modeling of Reactive Sputtering

Modeling of a reactive sputter process is important for the prediction of the properties of the resulting film. In this section, modeling of the reactive sputter process has been done for the case where Ta and Ti are reactively co-sputtered in an Ar/O_2 ambient (Paper VII). A slightly modified model has been developed for the description of the "baffled target" configuration (Paper VI). In both cases, simulations are based on extensions of Berg's reactive sputter model [35-44].

6.1.1 Reactive Magnetron Co-sputtering of Ta and Ti in an Ar/O_2 Ambient

The complex co-sputtering of Ta and Ti in an oxygen/argon environment was successfully simulated in Paper VII. The hysteresis region separating metal mode and compound mode sputtering can be found by varying the reactive gas flow and simultaneously monitoring e.g., target voltage, partial pressure of the reactive gas, or the deposition rate at the substrate. In this paper, the target voltage as a function of reactive gas flow was measured, and it correlates very well with simulated results of the deposition rate. It is demonstrated that the metal composition in the deposited film exhibits a hysteresis behavior as a consequence of the difference in reactivity at the two targets. This is shown in Figure 5, Paper VII.

6.1.2 Reactive Magnetron Sputtering of Ta Using the "Baffled target"- Setup

The simulations in Paper VI illustrate how the hysteresis effect in the reactive sputter process can be dramatically altered by "hiding" the target in a box having a small aperture, which also has been experimentally demonstrated by others [61-64]. It basically means that the target itself is secluded within an aluminum box, with an opening at the bottom having a direct line of sight with the substrate, thereby shielded from a direct contact with the incoming reactive gas. This setup is also schematically shown in Figure 23a. Berg's sputter model has been used as a starting point, and with the modifications made in Paper VI, it is shown to efficiently predict the "baffled target" behavior.

Following, is a description of the notation in Figure 23b. This is meant to give the reader a better understanding of the equilibrium balance equations, found in Paper VI, which are the basis for the model.

Θ_t – This is the fraction of the target covered with compound, thus the fraction from where compound particles are sputtered. Accordingly, $(1-\Theta_t)$ is the fraction of pure metal.

Θ_b – This is the fraction of inner walls in the box covered with compound.

Θ_s – This is the fraction on the substrate covered with compound material.

A_t, A_b, and A_s denote the area of the target, the inner walls of the box, and the substrate respectively.

R – This is the rate of either metal or compound sputtered from the target. Regardless of which rate discussed (metal or compound), one fraction stays inside the box and eventually adsorbs onto the box wall. The rest passes through the orifice into the main chamber, and most of it contributes to film growth on the substrate. The amount of particles that pass through the orifice depends of course on the size of the latter.

Γ - The flux of reactive gas molecules incident upon any surface in the system for a given partial pressure of reactive gas.

F_1 – This is the flux of compound molecules towards the metallic part of the box wall.

F_2 – This is the flux of metal towards the compound part of the box wall.

F_3 – This is the flux of metal atoms sputtered from the target, that pass through the orifice, towards the metal part of the substrate.

F_4 – The flux of compound material sputtered from the target onto the metal part of the substrate.

F_5 – The flux of compound material sputtered from the target towards the compound part of the substrate.

F_6 – This is the flux of metal from the target towards the compound part of the target.

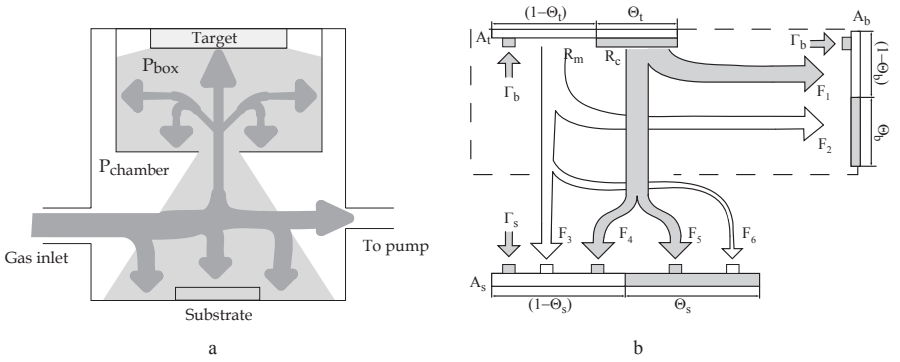

Figure 23. The figure shows the chamber setup during "baffled target" sputtering (a). The figure shown in (b) illustrates the sputtered fluxes and the coverage of pure metal as well as compound on the surfaces in the box and in the main chamber.

The implemented modified version follows in essence the same philosophy as in the standard model, and hence erects coupled steady state balance equations in the box as well as in the whole chamber. The resulting set of equations is then used for modeling of the process.

The aperture is the only channel for gas transport between the box and the main chamber. It efficiently limits the supply of reactive gas to the target surface, which significantly improves gettering within the box. It is shown that for small apertures, the target stays in metal mode even at high reactive gas flows. This enables deposition of a stoichiometric compound film with the target running in metal mode far away from the hysteresis region. It is also shown in Figure 7, Paper VI, that the latter is pushed towards higher reactive gas flows, and that a complete compound formation at the substrate is found farther away from the hysteresis region as the aperture size is reduced. This is also experimentally verified in Figure 8, Paper VI. It is found that stoichiometric films could be deposited in a very non-critical manner with respect to the hysteresis region.

6.2 Synthesis of Highly Oriented AlN Films

Ideally, monocrystalline materials are best suited for the fabrication of electroacoustic devices due to the low acoustic losses. The synthesis of epitaxial films, however, requires the use of special monocrystalline substrates as well as high temperature deposition processes. This will result in a substantially increased cost of the final device, hence render the technology unsuitable for mass production as well as incompatible with the IC-technology. Polycrystalline materials inherently yield higher losses due to intergranular reflections, losses due to the presence of voids and defects, surface scattering caused by the surface roughness, etc. On the other hand, synthesis of polycrystalline materials can be done with relative ease on almost arbitrary substrates and at a fraction of the cost, which is a big incentive to develop such synthesis methods and compare the properties of the polycrystalline materials with their monocrystalline counterparts.

In this work, AlN films have been synthesized by reactive sputter deposition. Two types of discharges have been explored, RF and pulsed DC sputtering respectively. It is shown that both methods are suitable for the deposition of high quality AlN films, which also is consistent with similar studies reported in the literature on both RF deposited [26, 28, 65-70] and DC deposited [27, 71-74] AlN films.

6.2.1 AlN Synthesis Using RF Reactive Magnetron Sputtering

Thin aluminum nitride films have been deposited on a variety of substrates; SiO_2, poly-Al(111), poly-Pt(111), Si(100), Si(111), polycrystalline diamond, sapphire [(001)α-Al_2O_3] and others. The films were systematically optimized as a function of the main deposition parameters such as process pressure, RF power, substrate temperature, and gas flow rate and composition with respect to film texture in view of obtaining highly c-axis oriented films.

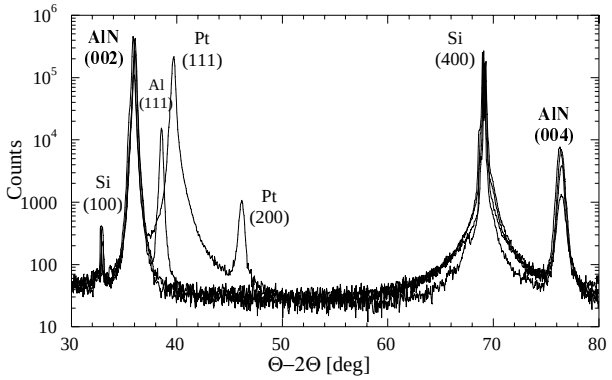

Figure 24. The figure shows a diffractogram for aluminum nitride films, approximately 2 μm thick, deposited onto Pt, Al, Si, and SiO_2. All the substrate peaks are identified except for the amorphous SiO_2, and the AlN peaks indicate an equally good film quality on all the substrates.

Initial studies indicated that both the roughness and the structure of the substrate material, along with the process parameters, played a significant role in the growth process. Rough substrate surfaces resulted in films with relatively poor texture, while smooth surfaces, using the same deposition parameters, resulted in highly oriented films. Thus, films deposited on thermally oxidized Si wafers exhibited a complete (0002) texture with a surface roughness of 8 Å, which is of the same order as for a polished Si surface [75]. The films were stoichiometric, with an oxygen content of less than 0.8 atomic-% according to ESCA analysis. The FWHM of the rocking curve was 1.6° for films deposited onto SiO_2. Figure 24 shows an XRD diffractogram of AlN grown at 350°C onto SiO_2, Al, Pt, and Si, and it is clear that all these substrates are suitable for growing highly oriented (002)-AlN at optimized growth conditions. The stress in the film was measured using an optical method and was estimated to be around –400 MPa.

In a parallel study, AlN films have also been grown on sapphire. As shown in Figure 6a, Paper III, films grown at a substrate temperature of 500°C are epitaxial, which is one of the lowest temperatures reported in the literature for epitaxial AlN films. The films had a rocking curve value of 0.4° which compared to related studies [19, 76, 77] is rather good considering the moderate deposition temperature. The dislocation density estimated from TEM observations shown in Figure 7, Paper III, was $10^{11}/cm^2$, which can be lowered significantly by using other techniques at higher temperatures [78]. It should be noted that epitaxial AlN films have been deposited at even lower temperatures by *Shiosaki et al*. [79], however, those films exhibit rather large FWHM rocking curve values. At higher temperatures, FWHM rocking curve values below 0.03° have been reported [80].

The main conclusion from this part of the work is that reactive sputter deposition, being a plasma assisted process, provides enough energy to the growing film through ion and electron bombardment, which facilitates crystalline growth at low temperatures, which in turn is an objective in this work.

6.2.2 AlN Synthesis Using Pulsed DC Reactive Magnetron Sputtering

The main advantages of pulsed DC sputtering over RF sputtering are the higher deposition rate as well as the simplicity of the process - RF power supplies are more complex and expensive, not readily scalable, more hazardous, require a tuning network, etc. For this reason, a significant part of the synthesis work focused on pulsed DC sputter deposition.

Synthesis of AlN films with pulsed DC reactive magnetron sputtering has been mainly done on Si(100), Si(111), poly-Al(111) and SiO_2 substrates as shown in Paper V and IX. The process parameters such as process pressure, DC power, duty cycle, pulse frequency, substrate temperature, and gas flows have been optimized with respect to film texture. The films obtained in the DC configuration are highly (002)-oriented with a very low oxygen impurity concentration of 0.5 atomic-% and a rocking curve FWHM of 1.6°.

Perhaps, one of the major achievements in this part of the work is the identification of the so-called Atom Assisted Deposition (AAD) process. The essence of the latter is as follows. It is well known that growth at low temperature results in the deposition of either amorphous films or at best polycrystalline films with rather poor texture due to the low surface mobility of the condensing species on the surface. For this purpose most PVD processes use additional energy sources, most typically from ion and/or electron bombardment. This is normally done by applying a negative bias to the substrate holder, which increases the energy of the bombarding ions from the plasma. Another possible energy source could result, under specific circumstances, from energetic atoms that are in fact reflected ions off the target and subsequently neutralized. These neutrals are not affected by the electric field between the electrodes and, provided they are not scattered substantially in the gas phase, deliver substantial energy to the growing film. On the other hand, these neutrals are relatively few (depending on the reflection coefficient) but possess high energy, which causes resputtering of the growing films as well as substantial structural damage, for which reason it is often

considered as an undesirable effect. In the light of this, the AAD process can be explained as follows. It is well known that the energy distribution of the sputtered atoms exhibits a maximum centered at around half the sublimation energy of the target and then tails off as E^{-2} with energy. The conclusion from this is that the average sputtered atom has a kinetic energy which is in the range of several eV, the thermal equivalent of which is a thousand degrees or more. Unfortunately, in normal processing conditions (process pressure and target to substrate distance) these sputtered atoms are quickly thermalized through gas phase collisions and hence condense onto the surface of the growing film with thermal energy equal to that of the ambient (room temperature). Modern sputter magnetrons, on the other hand, have sufficiently strong magnetic field to sustain the discharge at relatively low pressures, i.e. down to 1 mTorr is not unusual. Thus, a pressure of 1 mTorr and a target to substrate distance of 6 cm would result according to equation (3), in that most of the sputtered atoms will arrive at the substrate without experiencing gas phase collisions. In other words the very condensing species arrive with sufficient kinetic energy to promote surface diffusion and crystalline growth. This is exactly the essence of the AAD process. By way of example, Figure 25 shows the (002) FWHM of the rocking curve and the deposition rate for AlN films grown at various process pressures. It is seen, that at pressures above 6 mTorr the films have extremely poor texture. In addition, the Θ-2Θ diffractogram (not shown here) exhibits several other than the (002) peak. On the other hand, the films deposited at pressures below 2 mTorr exhibit excellent texture and are fully c-axis oriented, which is primarily due to the AAD process. It should be emphasized that the contribution of fast neutrals in the above process should not be neglected and it certainly plays some role, since the reflection coefficient for N ions from an Al target at an energy of 150 eV is around 0.08, which indicates that the film is also bombarded by energetic N neutrals.

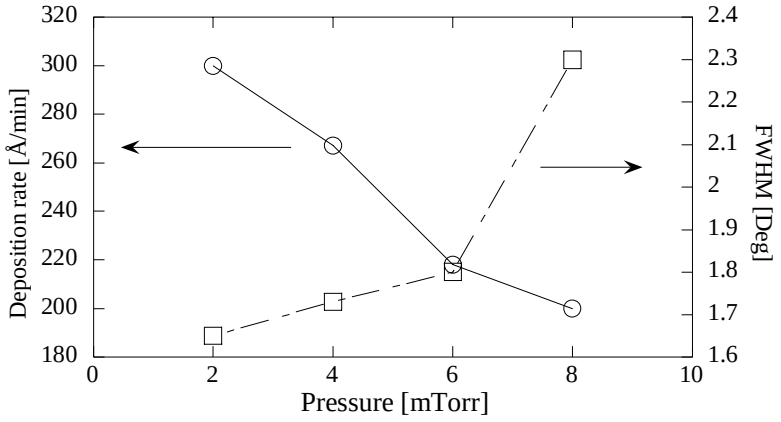

Figure 25. The figure shows both the deposition rate and FWHM of the rocking curve as a function of process pressure for AlN.

Further, as argued above, the control of the residual stress in the films is of great importance for electroacoustic devices. In this respect, Paper IX studies in great detail stress evolution as a function of the main process parameters. It is shown that the residual stress in (002)-oriented polycrystalline AlN grown on Si(100) substrates is greatly affected by the latter, and the stress evolution generally exhibit a transition from compressive to tensile depending on the parameter varied. This is illustrated in Figure 26, which shows the residual stress in the films as a function of process pressure.

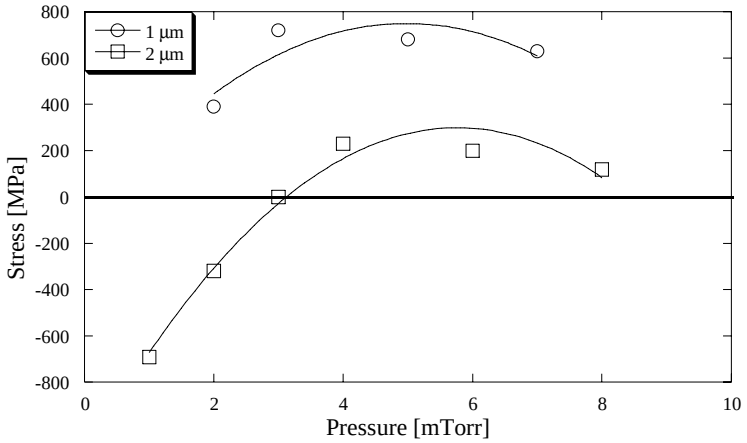

Figure 26. The residual stress in AlN films as a function of process pressure for two different film thicknesses as measured using an optical method.

The major mechanism responsible for stress evolution in the film is shown to be peening [49, 81, 82] and atom assisted deposition, both of which deliver kinetic energy to the growing film. Further, increasing the temperature above 400°C during deposition resulted in films exhibiting a significant increase in thermally induced stress, due to the difference in thermal expansion of the materials. The temperature dependence for the thermal expansion of AlN and Si is shown in Figure 6, Paper IX. It is seen in the latter that a process temperature above 400°C gives rise to a significant thermal stress.

6.3 Electrical Characterization

Electrical characterization has been made on AlN MIM and MIS structures, as well as on $(Ta_2O_5)_{1-x}(TiO_2)_x$ MIS structures. These studies provide information about the leakage current behavior as well as the dielectric characteristics of the films from simple test structures. It is desirable that the test structure dependence as a function of temperature and frequency is weak, or at least predictable, for the final device to be reliable in an IC-system.

6.3.1 Electrical Characterization of AlN

Electrical characterization was done on MIM and MIS structures fabricated from both highly (002)-oriented as well as x-ray amorphous AlN thin films. In Paper VIII it is shown that the leakage current mechanism through the films is of Frenkel-Poole type, explained by field enhanced thermal excitation of trapped charge carriers into the conduction band. The activation energy for the traps is calculated to be 0.6 eV. The dielectric constant as calculated from CV measurements was 10, which is consistent with values reported by others [31, 83-85]. The dielectric constant was also shown to be independent of the degree of crystallographic orientation in the film. In addition, heat treating the samples in an N_2/H_2 environment for 30 minutes did not yield any detectable effect on the dielectric behavior.

Further, high frequency measurements were done on capacitor structures of different sizes for frequencies up to 10 GHz. The dielectric constant was stable, and showed no tendency to deviate from the low frequency value in the measured frequency range. The dielectric loss tangent was measured to lie below 0.03 in the same frequency interval. This is in accordance with the results obtained by *Dimitrova et. al.* [84], although a bit higher than what has been found by *Noreika et. al.* [31]

From the electrical measurements it could be concluded that the charge traps are confined to a thin layer at the AlN/Si interface, because of the linear relation between the flat band voltage and the film thickness (Figure 2, Paper XIII). The IC-compatibility of AlN together with the low leakage current and the dielectric properties obtained in this investigation place AlN as a possible candidate for a gate dielectric in MOS technology.

6.3.2 Electrical Characterization of $(Ta_2O_5)_{1-x}(TiO_2)_x$

The electrical characterization was done on MIS structures, consisting of $(Ta_2O_5)_{1-x}(TiO_2)_x$ films (where x varies in the range 0-0.4) deposited onto n-doped Si(111) wafers. The as deposited film does not show the typical CV behavior of a dielectric thin film, which is a consequence of a very large amount of charges in the oxide. As films are heat treated in Ar, the amount of mobile charges is decreased, and the film treated at 600°C had a nicely shaped CV curve with a flat band voltage of 0.2 V. At 800°C, the film turns crystalline, and the CV curve shows a hysteresis behavior similar in shape to what has been observed in the case of AlN. The hysteresis is believed to be caused by the existence of charge traps in either the oxide or the interface that are charged/discharged when the voltage is swept back and forth. Further, the Ti doped films treated at 800°C exhibit a significant increase in the dielectric constant from about 20 to 30, due to increased polarization of the crystalline phase. However, these values for the dielectric constant are not as high as those reported by *Cava et. al.* [86], although the results in the latter reference have been obtained from bulk ceramics. Interestingly enough, the films that are not doped with Ti, exhibit a relatively stable dielectric constant of approximately 20 in the entire temperature range.

The leakage current stays more or less constant in films heat treated up to 600°C, whereas the current in the films treated at 800°C increases and reaches

unacceptable levels. Other gases used during the heat treatment have also been reported to affect the dielectric constant, and both O_2 and N_2 [87] are shown to decrease the leakage current through the film. As opposed to that, O_2 has also been shown to increase the leakage current [88].

6.4 Etching

Etching of III-V semiconductors is very challenging due to their strong bonding energy. As a matter of fact, among the III-V materials of interest for electronic devices, AlN has the highest bonding energy of 11.52 eV/atom as compared to 8.92 eV/atom and 7.72 eV/atom for GaN and InN respectively [89]. In this investigation, etching of Al and AlN was done in an ICP reactor using a chlorine based chemistry. Optimization of the Al and AlN etch process was done primarily to find a recipe intended for the fabrication of resonant structures, SAW and BAW filters. Since the structures are fundamentally different, it is advantageous to be able to greatly affect the etch rate by modifying the process. It is noted that for the fabrication of SAW resonators it is desirable to have a high etch rate for Al, whereas the etch rate for AlN should be kept as low as possible. On the other hand, for the fabrication of BAW resonators, it is desirable that it is the other way around.

Etching of Ta_2O_5 was done in a fluorine based chemistry. The recipe for Ta_2O_5 etching was primarily developed to achieve suitable process parameters for the patterning of integrated capacitor structures.

6.4.1 Aluminum

Etching of Al in a chlorine based chemistry is generally a fast process, and very dependent on the concentration of chlorine radicals available in the chamber. The process, where Al and Cl radicals react to form $AlCl_3$ or Al_2Cl_6, followed by desorption from the surface, is spontaneous [90, 91], and thus purely chemical. Both reaction products mentioned are possible, although the formation of Al_2Cl_6 is the more probable event [89] at the temperatures in question. The spontaneous nature of Al etching means that sidewall passivation is necessary to maintain the line width. To decrease the lateral etch component small amounts of oxygen are added to the process as shown in Paper IV. This leads to the formation of the chemically very stable Al_2O_3 compound on the sidewall surfaces. In addition, the oxygen helps to increase the concentration of chlorine radicals in the plasma. Hence, the etch rate of Al increases up to a point where dilution and alumina formation become the dominant reaction processes. In Paper IV aluminum etch rates of about 1 μm/min were obtained, while at the same time the selectivity of Al towards AlN was as high as 1000 as shown in Figure 7 in the same paper. Recalling Figure 2a showing the SAW filter structure, it is easy to realize that such a high selectivity is satisfactory for patterning the Al top electrode (IDT), leaving the exposed AlN virtually unaffected. The largest Al etch rate observed was 1.8 μm/min.

6.4.2 Aluminum Nitride

As a step in the fabrication of a BAW resonator one needs to open a contact to the bottom electrode through the active AlN film (see Figure 3). Etching of AlN was done in an ICP reactor using a chlorine chemistry based on Cl_2 and BCl_3, and was found in Paper IV to be a relatively slow process. It is noted that AlN does not react spontaneously with Cl radicals, which necessitates the use of ion bombardment to break the strong Al-N bond, followed subsequently by the formation of Al_2Cl_6. The latter together with the nitrogen is removed via the system exhaust. The etch rate of AlN ranges from values close to zero up to 90 nm/min depending on the energy of the bombarding ions, although etch rates of around 0.8 μm/min have been obtained by others [92].

Fluorine is generally not used for etching of III-V materials, since the generated fluorides very often are non-volatile, thus passivating the surface. However, it has been observed by *Shul et. al*. [14] that 20% SF_6 in the feed gas seems to enhance dissociation of BCl_3 resulting in an increased concentration of Cl radicals. Nevertheless, higher concentration of SF_6 had a negative impact on the etch rate due to passivation of the substrate surface. Al is the most suitable electrode material (high mechanical Q and low resistivity) but it cannot be used as a bottom electrode due to the poor selectivity of the above process. For this purpose, Pt and Mo have been used for the formation of the bottom electrode of BAW resonators.

6.4.3 Ta_2O_5

Etching of Ta_2O_5 was done in an ICP system using a polymerizing chemistry based on CHF_3, which dissociates in the plasma and forms various CF_x radicals and atomic fluorine. The CF_x radicals tend to deposit onto the surrounding surfaces and form a polymer film. The addition of small amounts of oxygen and the use of ion bombardment at the same time by applying bias to substrate holder removes this film from surfaces exposed to the ion flux (the bottom of the grooves) which results in a highly anisotropic process. Fluorine reacts with Ta to form TaF_5 which is volatile at 230°C, and oxygen ions react with the polymer film to from CO, CO_2, and COF_2. The polymeric layer that forms onto the substrate thus plays an important role in the process, and its thickness correlates strongly with the etch rate as shown in Figure 5, Paper II. Further, the temperature of the surrounding chamber walls are also shown to influence the etch process. As the temperature on the walls increases, the concentration of polymer forming species in the gas phase increases, thus etch rates are reduced. The selectivity between Ta_2O_5 and poly-Si (a possible alternative as the bottom electrode) was estimated to be close to 5, which is sufficient for the fabrication of the complete MIS structure.

6.5 Electroacoustic Characterization of AlN

Electroacoustic characterization of the AlN films is the last major objective of this work. It has been done by measuring the frequency response of thin film SAW and BAW resonators as well as transversal SAW filters. The design of the latter has been optimized using several computer models as indicated above. Thus for SAW resonators the program LAYERS was used to find the dispersion curves of

the electromechanical coupling and of the phase velocity as a function of thickness of the AlN film, frequency and direction of propagation in the Si substrate. From these dispersion curves one readily derives the optimal layered structures in view of obtaining high electromechanical coupling. Finally, the electroacoustic characteristics were extracted using the COM model.

BAW resonators, on the other hand, were first simulated with the Nowotny-Benes model [58, 59] to find the most suitable electrode thickness and center frequency. Consequently, the electroacoustic properties in the c-direction were derived from analysis of the frequency response of the resonators.

6.5.1 SAW Resonators

In order to test the resonator technology first, SAW resonators on single crystalline quartz have been initially fabricated. Quartz is one of the best materials for electroacoustic applications at low frequencies and is well characterized. Some of its best properties are its extremely high thermal stability for certain cuts as well as its high mechanical Q, which is of the order of $7 \cdot 10^6$ @ 1 MHz [93] for premium grade quartz. This value is of course reduced in a loaded resonator, although Q-values of several hundreds of thousands is not unusual, which is orders of magnitude better than the best performing LC circuit. The disadvantage using quartz is its relatively low coupling coefficient, and the fact that using a bulk material disables the flexibility of thin film technology.

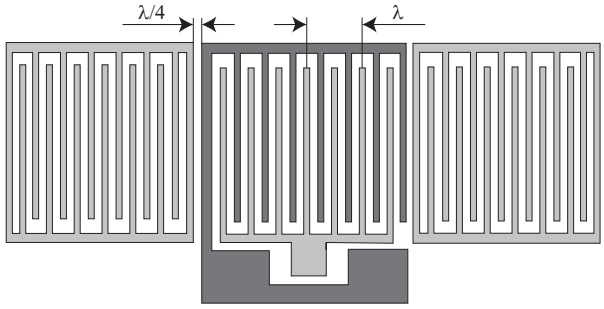

Figure 27. The figure illustrates the SAW resonator, consisting of an IDT surrounded by two reflectors. The distance between the IDT and the reflector is λ/4. The reflector can be either grounded or "floating" depending on the application.

A typical synchronous SAW resonator consists of an interdigital transducer surrounded by two reflectors which consist of linear metal stripes with the same period and width as the IDT. The reflectors are normally grounded and are located at a distance λ/4 from the IDT as shown in Figure 27.

In this work the reflectors and the ITDs were fabricated in one and the same lithographic step, most of them being made with a standard mask and a wavelength of 10 μm. The quartz resonator frequency response was measured by a Network Analyzer (HP 8720D) in a one port configuration and the results are shown in Figure 28. The resonator was fabricated on ST-cut quartz. The sharp resonant response at a frequency of 313 MHz indicates a large Q-value, and for this

particular device, it was estimated to be about 6000 using equation (10), where f_r is the center frequency and Δf_r is the FWHM of the conductance peak at resonance. Note that the Q-value is normally given as a product with the operating frequency. Thus, these particular measurements yield a Q-value of $6000 \cdot 313 \cdot 10^6 = 1.9 \cdot 10^{12}$ Hz, which value is not very different from the one quoted above. The coupling coefficient has been measured using a fitting method, and was found to be about 0.11%.

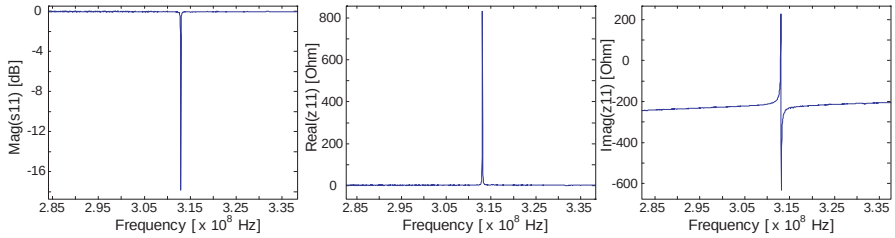

Figure 28. The frequency response of a quartz resonator; s11, real part of the impedance, and imaginary part of the impedance.

Further, AlN thin film SAW resonators on Si substrates have been fabricated. The layered structure consisted of 2 μm thick AlN, 0.7 μm thick SiO_2 onto Si(100). The wave propagation was in the (110) direction in the Si substrate at a wavelength of 10 μm. Figure 29 and 30 shows the response from two such resonators, deposited on a moderately doped silicon (≈ 1-5 Ωcm) wafer and a very high resistivity (≈ 15000 Ωcm) silicon wafer respectively. It is seen that the loss in the latter case is significantly lower than for the low resistive case, depending on the capacitive coupling through the substrate giving rise to substrate currents. The center frequency of close to 470 MHz yields a SAW velocity of 4700 m/s. The large capacitive coupling to the substrate, however, did not allow accurate measurements of the Q-factor and the coupling coefficient. Nevertheless, these experiments indicated that AlN thin film SAW resonators on Si exhibit a relatively high acoustic velocity and hence can operate at relatively high frequency for the same wavelength.

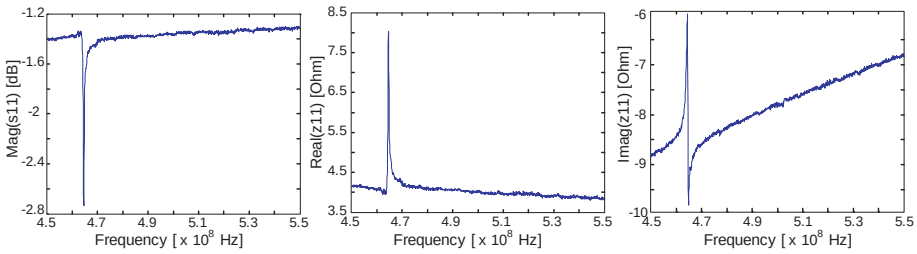

Figure 29. The frequency response of an aluminum nitride resonator grown on SiO_2/Si substrates, with the silicon moderately doped; s11, real part of the impedance, and imaginary part of the impedance.

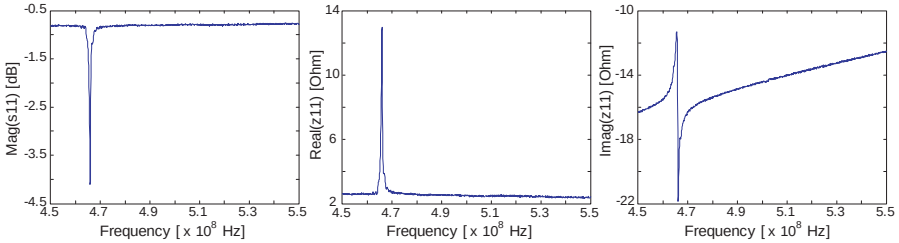

Figure 30. The frequency response of an aluminum nitride resonator grown on SiO_2/Si substrates, with the Si highly resistive; s11, real part of the impedance, and imaginary part of the impedance.

Finally, to really exemplify the advantages of thin film electroacoustic devices, similar AlN FSAW resonators were fabricated on polycrystalline diamond. The latter is in fact deposited by a CVD method onto a Si substrate with a thickness of 50 μm. It is noted that in this case the Si substrate does not influence the wave propagation since the SAW wave penetrates down to a depth of 2 wavelengths beneath the surface. Diamond was chosen due to its high acoustic velocity, and hence the combination of a piezoelectric film with a fast substrate allows the fabrication of high frequency SAW devices.

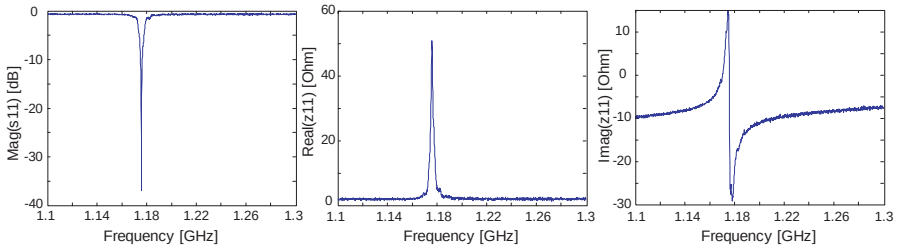

Figure 31. The frequency response from an aluminum nitride resonator grown on polycrystalline diamond; s11, real part of the impedance, and imaginary part of the impedance.

This is clearly demonstrated in Figure 31, which shows the frequency response of AlN/Diamond FSAW. The first thing to be noted is the resonant frequency which is 1.18 GHz, i.e. more than two times higher as compared with the previous case, and yields a SAW velocity of around 11800 m/s. In other words, 10 μm wavelength corresponds to a lithography resolution of 2.5 μm. This means that with a relatively standard lithography resolution of 0.5 μm FSAW acoustic devices operating with frequencies at around 6 GHz are readily achievable. It is noted that no existing single crystalline piezoelectric material can yield such a frequency at the same wavelength, since the SAW velocity in most common piezoelectric materials is between 3000 and 4000 m/s. Further, from the frequency response in Figure 31 the major electroacoustic parameters have been derived using the COM model. Thus, the electromechanical coupling was estimated to be 1.14% which is a reasonably high value and in agreement with theoretical calculations. A Q-factor of 600 has been measured which is sufficiently high for SAW devices.

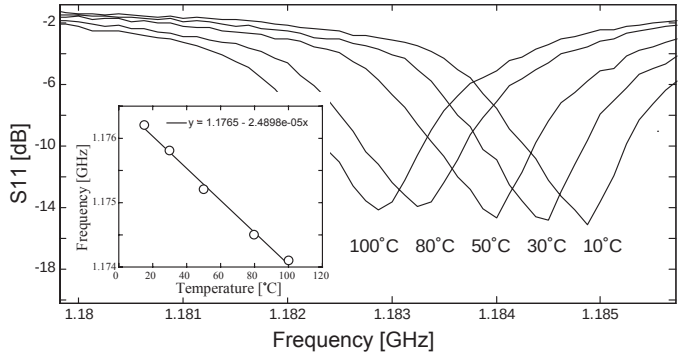

Figure 32. The resonance frequency of an AlN/Diamond SAW is shifted as a function of the temperature. The inserted figure shows the linear dependence between the resonance frequency and the temperature.

Finally, the temperature coefficient of delay has also been measured in the temperature range 10°C to 100°C as shown in Figure 32. The value of -18 ppm/K is consistent with that for pure AlN, which is around -25 ppm/K (see below).

6.5.2 BAW Resonators

BAW resonators are another type of electroacoustic devices where the acoustic wave propagates in the bulk of the material and hence its performance is largely dependent on the properties and the quality of the material, provided that the contribution from the electrodes is taken into account. That is why they are ideally suited for the characterization of the quality of the deposited films.

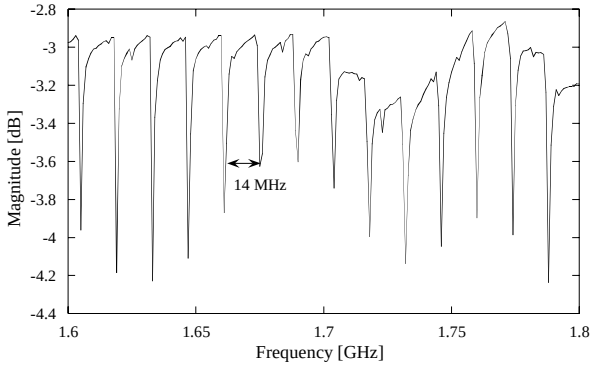

Figure 33. The frequency response of a BAW before the membrane is released by dry etching the Si substrate from the backside.

Thin film bulk acoustic resonators (TFBAR) were fabricated using well-established semiconductor processes on 4-inch double polished silicon wafers, as illustrated schematically in Figure 22. A 1.7 μm thick highly oriented c-axis AlN film defines the active piezoelectric layer sandwiched between a Mo bottom

electrode and an Al top electrode, both 300 nm thick. The reason for using Mo as bottom electrode is the good etch selectivity during etching of AlN for opening contact holes. In addition, a 1.7 μm thick amorphous AlN was grown between the resonator and the Si substrate, and which layer was used as both an etch stop layer during the back etch of the Si substrate and as a supporting layer to increase the mechanical strength of the structure. Thus, the total thickness of the resonator was 4.0 μm and had an area of 0.01 mm^2. These dimensions were chosen such that the impedance of the device was approximately 50 ohms at resonance.

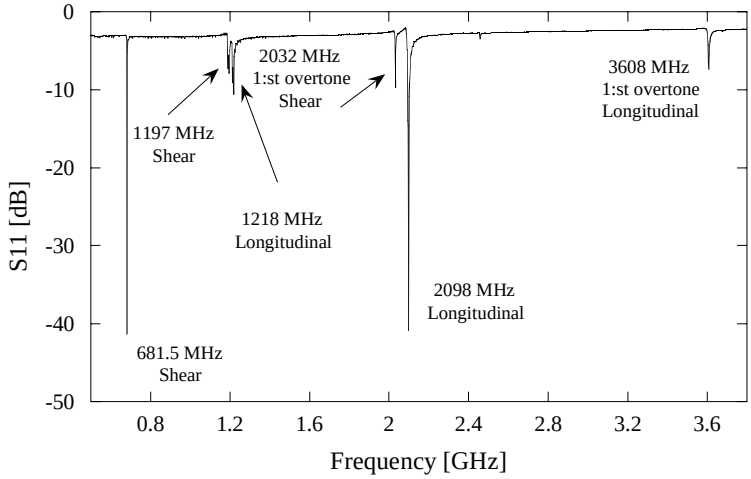

Figure 34. The frequency response of a membrane type BAW after the silicon has been removed.

One port measurements were then performed to characterize the TFBAR's. Data was collected both before and after the backside etch of the wafer. It is noted that before the backside etch, the silicon substrate acts as a low loss acoustic cavity and the whole device operates as a high overtone TFBAR resonator. The latter exhibit a series of overtone resonances with frequency separation between the peaks given by equation (11) [3]

$$\Delta f = \frac{v_a}{(d'+d)} \quad d >> d' \tag{11}$$

Figure 33 shows the frequency response of the device before the etching. Assuming a phase velocity of 8430 m/s for silicon, equation (11) yields a frequency separation of 13.9 MHz, which is in excellent agreement with the measured separation of 14 MHz.

After etching the Si substrate, the device operates as a standard FBAR resonator and its frequency response is shown in Figure 34. The resonator was also modeled with the Nowotny-Benes [58, 59] model and a comparison between the calculated and measured results are shown in Table 1.

Table 1. Calculated and measured values of the resonance frequencies for longitudinal and shear mode waves for a membrane BAW.

Acoustic path Length [μm]	f_{calc} long. [MHz]	f_{meas} long. [MHz]	f_{calc} shear [MHz]	f_{meas} shear [MHz]
3.95	1230	1218	675	681
2.25	2102	2098	1184	1197

The small difference between calculated and measured results are readily explained by thickness variations in the both the electrode layers as well as in the active AlN film.

Further, high resolution scans of the fundamental resonance frequency at 681 MHz is shown in Figure 35. The Figures clearly show that there are multiple resonances around the fundamental frequency, which can be explained by lateral excitation of low frequency modes in the resonator. Consequently, high order harmonics of these modes appear in the main resonance as spurious responses. The latter can be efficiently suppressed by using electrodes with non-parallel sides [94].

A coupling coefficient of ~5% and a Q-value of ~1600 was calculated using equation (9) and (10) respectively for the resonance at 681 MHz, where f_a and f_r are the resonant and anti-resonant frequencies respectively. The same calculation for the fundamental mode at 2098 MHz was not possible, due to the strong perturbation from spurious modes.

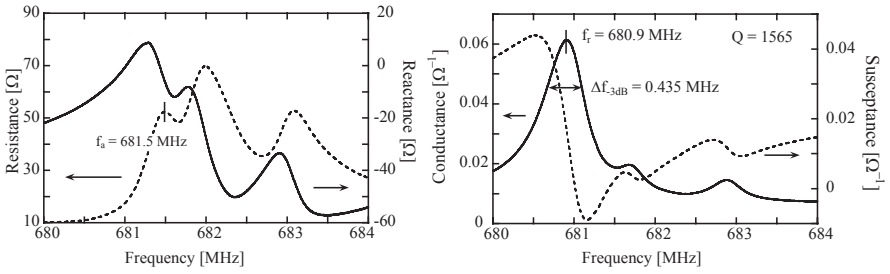

Figure 35. The impedance and the admittance for the shear mode resonance at 681.5 MHz is shown. The real parts are used to calculate the coupling coefficient and the Q-value.

The temperature coefficient of frequency was measured by mapping the reactance of the lower frequency shear mode (681 MHz) at three different temperatures, 22°C (RT), 60°C, and 100°C. This is shown in Figure 36, and as expected, the resonance frequency decreases in a linear manner with temperature, which is also seen in the inserted graph in the Figure. Equation (12) has been used

to calculate the temperature coefficient to be –31ppm/°C for the shear mode, and –24 ppm/°C for the longitudinal mode with its resonance at 2098 MHz, which is in accordance with results obtained in by other researchers [95].

$$\frac{df_r / dT}{f_r^{RT}} \quad [ppm/°C] \tag{12}$$

In addition, the resonance frequency is inversely proportional to the square root of the characteristic capacitance in the structure, which in Paper VIII is shown to increase as a function of temperature. This also supports the decrease in resonance frequency with temperature.

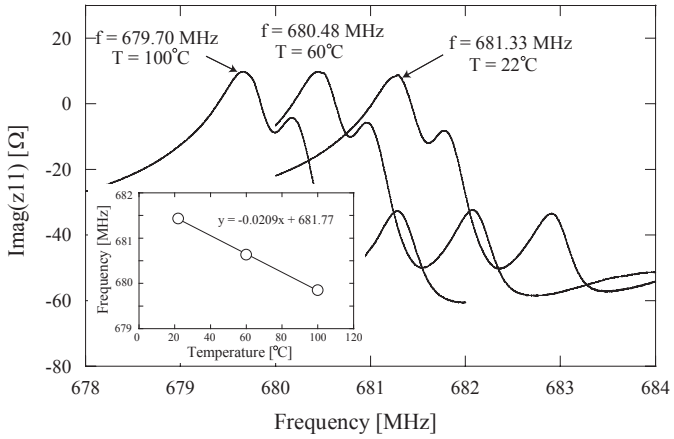

Figure 36. This figure shows how the resonance frequency of an FBAR is shifted as a function of the temperature. The inserted figure shows the linear dependence between the resonance frequency and the temperature.

6.5.3 SAW Filter Structures

Complete transversal AlN SAW test filter structures, schematically illustrated in Figure 2a, was fabricated and electrically evaluated. Our best performing filters had an oxygen content lower than 0.5% (Paper I), and it has been shown that the increase of oxygen in the film results in a weakening of the (002) peak intensity [4, 96]. This is also reflected in an increase of the insertion loss of the filter [96]. Figure 37 shows a mismatch compensated filter response from a transversal SAW filter, having a center frequency of 0.549 GHz. The phase shift of the same filter, shown to be linear as theoretically predicted, is also shown in the same figure. The side lobe suppression is approximately 11.5 dB, which is sufficient for discrepancy of the filter response from the rest of the spectra. The coupling coefficient was calculated to be 0.37%. Insertion loss for the mismatch compensated filter was measured to be 16 dB, of which the propagation loss was estimated to be about 4.7 dB/cm in accordance with work made by others at the frequencies in question [10, 96, 97]. The phase velocity of the SAW wave mode was 4900 m/s with a wavelength of 9 μm.

Recently, interesting SAW results have been obtained by growing single crystalline GaN onto (0001)-sapphire, showing a phase velocity of 5803 m/s, coupling coefficient as high as 4.3% and an insertion loss of only 7.7 dB [98].

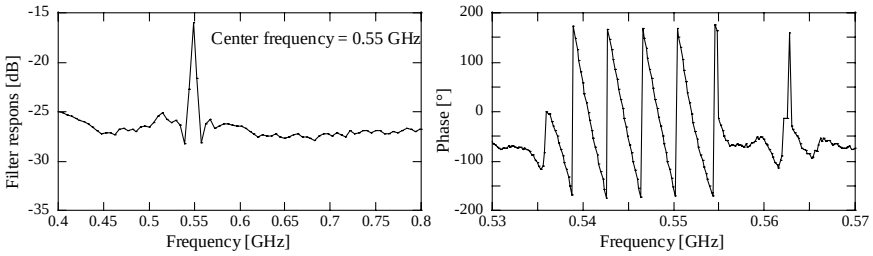

Figure 37. Filter response and phase for a transversal SAW.

7 Summary of Papers

Paper I

The growth of polycrystalline AlN thin films on thermally grown SiO_2 using RF reactive sputtering has been systematically studied. The films have been optimized with respect to RF power, Ar/N_2 ratio, process pressure, and substrate temperature. It is found that properties such as the degree of orientation, crystallite size, surface roughness, stress etc. all are very sensitive to the deposition parameters. The films deposited at optimal deposition parameters were shown to be of very high quality with the c-axis perpendicular to the substrate surface. Further, to study the electroacoustic properties of the films, thin film transversal test structures consisting of non-apodized Al interdigital transducers formed on $AlN/SiO_2/Si$ were fabricated and evaluated with a network analyser. The measurements indicated a SAW velocity of 4900 m/s, propagation losses of 4.7 dB/cm and an electromechanical coupling of 0.37%.

Paper II

Integrated capacitors cover a large fraction of the total chip area in today's semiconductor industry. By using a material with a large dielectric constant, this area can be significantly reduced. One such material is Ta_2O_5, a so called high epsilon material with a dielectric constant of about 25, which can be increased even further with doping it with Ti. In this paper, etching of Ta_2O_5 has been done in an ICP system, using a polymerizing chemistry, and it has been shown that the deposition of fluorocarbon containing species plays an important role in the process. Also the temperature of the substrate as well as of the surrounding chamber walls greatly affect the process. Principally, the process pressure and the substrate bias were systematically studied, to find process conditions with sufficient selectivities. It was found that the process could be used to successfully fabricate a complete test structure.

Paper III

In this Paper, AlN thin films were deposited in an Ar/N_2 mixture on several different substrates by using radio frequency (RF) reactive sputtering. The structural properties of the films were optimized by systematically varying deposition parameters such as process pressure, gas mixture, substrate temperature, and discharge power. It was found that all the substrates used in this investigation resulted in films of very high quality with a complete (002)-orientation, provided that the substrate surface was sufficiently smooth. The films deposited on sapphire were epitaxial despite the relatively low deposition temperature of 500^oC, and showed a FWHM of the (002) rocking curve of 0.4°. The surface of the grown films was very smooth in the same range as a polished silicon surface. This indicates a high surface mobility of the atoms during film growth.

Paper IV

Metallization is a very critical step in the fabrication of high frequency Al/AlN/Substrate thin film based surface acoustic wave devices. The AlN surface in such applications is extremely sensitive to both particles from the lithography, as well as ion induced damage from the etch process. In this Paper, etching properties such as etch rate and selectivity between the materials of interest was studied. The goal was to find a recipe that etches Al very fast, while having at the same time a very high selectivity with respect to the underlying AlN film. The starting point was a Cl based chemistry with the addition of O_2 to slow down the lateral etch component. The dominant etch mechanism for the removal of Al was found to be ion assisted chemical etching, whereas the main mechanism for the AlN etch was predominantly physical sputtering. Thus, process parameters resulting in a very high selectivity between Al and AlN could be found by keeping the applied bias at a sufficiently low value. Hence, Al/AlN/Substrate structures with perfect Al pattern delineation and an intact AlN surface could be realized.

Paper V

The deposition temperature of a specific film is very important in IC-fabrication since it may affect the rest of the device in an undesirable and sometimes detrimental way. One of the most likely ways for integrating the thin film electroacoustic technology with the IC-technology is back end integration, which by obvious reasons allows a rather low thermal budget for the electroacoustic component. This necessitates the development of low temperature deposition processes of the piezoelectric film and which is the main focus of this paper, namely low temperature synthesis of highly textured AlN thin films with pulsed DC sputtering. To achieve this we studied systematically the influence of the major process parameters on the film texture. It was found that the process pressure had a profound effect on the film texture as it determines the deposition rate, the energy and direction of the condensing Al atoms, the impurity incorporation into the film, and hence influences significantly the film properties. It was found that at pressures below 2 mTorr, the films had an excellent (002) orientation as well as very good electroacoustic properties. One major mechanism responsible for the textured growth at such low temperatures, as argued in the paper, is considered to be atom assisted deposition. The latter term denotes that the Al species are themselves energetic as they arrive at the substrate surface, due to insignificant energy losses in gas phase collisions and hence provide enough kinetic energy to the growing film to stimulate surface diffusion and hence crystal growth.

Paper VI

Modeling is a powerful instrument for predicting the behavior of processes. By modeling, as well as process simulation, both time and effort can be saved leading to efficient research. This paper deals with both theoretical and experimental studies of reactive sputtering with the target semi isolated from the rest of the chamber by an aluminum box. The only connection between the main chamber and

the target inside the box is an orifice with a well-defined opening. This implies that gettering inside the box is extremely efficient resulting in a much lower partial pressure of the reactive gas as compared to its partial pressure in the main chamber. The simulations indicated that by using this technique, the hysteresis region for the target can be pushed towards significantly higher gas flows. These predictions have been confirmed by experiments, which show that fully stoichiometric films can be deposited in a very non-critical manner far away from the hysteresis region.

Paper VII

Materials with a high dielectric constant are of great interest for the next generation of gate dielectrics. It has been shown that Ta_2O_5 seems to have very attractive dielectric properties making it a possible candidate as a gate material. Further, its dielectric constant of 25 can be increased by the addition of small amounts of Ti. In this paper, the deposition process of stoichiometric Ta_2O_5 by pulsed DC dual magnetron sputtering was studied both theoretically and experimentally. Deposited films with TiO_2 concentrations between 0-40% have been electrically characterized. The films with a moderate incorporation of Ti exhibited an increase in dielectric constant after crystallization in a high temperature annealing step. The annealing also resulted in a significant increase in the leakage current due to current paths along the grain boundaries. This study shows that Ta_2O_5 is very attractive for the replacement of SiO_2. However, no significant improvement of the electrical properties of Ta_2O_5 could be detected by the addition of small amounts of Ti.

Paper VIII

In this paper, both MIS and MIM structures based on amorphous and polycrystalline reactively sputtered AlN films have been electrically evaluated. The crystalline films were highly (002) oriented with the c-axis perpendicular to the substrate surface. CV measurements revealed a very stable dielectric constant of 10 regardless of the crystallinity of the film (including amorphous). Additional dielectric measurements using a network analyzer showed that the dielectric constant was also very stable with frequency up to 10 GHz. Leakage currents trough the AlN film were found to be Poole-Frenkel controlled, and hence thermally activated. The properties of the AlN as determined from these studies indicated that the material is very promising for integrated capacitors and possibly as a gate dielectric.

Paper IX

In this paper, a systematic study of the residual stress in fully textured AlN films during reactive sputter deposition has been performed. The stress in oriented polycrystalline AlN films is often substantial, and may affect significantly the performance of AlN based electroacoustic devices. It is found that all the major deposition parameters, such as process pressure, gas flow, substrate bias, and discharge power affect substantially the residual stress in the films. It is also argued

that the major mechanism responsible for stress evolution in the films are atom assisted deposition and atomic peening. It is shown that the stresses can be controlled by the deposition parameters, and that stress free films can be deposited at room temperature at optimized conditions.

Acknowledgement

When I first started out my studies at Civilingenjörsutbildningen, it was definitely NOT my intention to eventually summarize the past sixth of my life writing a thesis. It was more like an experiment, aiming to find out what kind of human beings that actually volunteer to spend another, at least, 4½ years studying when compulsory school and gymnasium finally was over. The result was as unexpected as it was striking – I found a whole bunch of "hygglo" people that made those years run by with an infinite number of laughs. After finishing Civilingenjörsutbildningen I once again faced the same situation as 4½ years earlier, although this time I was no longer a rookie, and didn't hesitate to continue my experimental studies for another couple of years.

Looking back, I can honestly say that I wouldn't have made it to this point without the help from all the people around me, both inside and outside the University, and I owe a debt of gratitude to all of you!

So, in no specific order…

I especially would like to express my sincere gratitude to Professor Sören Berg, who despite the fact that he SAW ☺ the miserable results my x-jobb concluded into, gave me a desk, computer, supervisor, and via the "never ending smiler" Ingrid Ringård an "anställningsavtal".

That brings me to my supervisor, Ilia Katardjiev, who constantly impress on me with his inexhaustible source of knowledge and the speed at which he absorbs information. You have always had time to help when the water was too deep, or too shallow for that matter - THANK YOU!!!

Another person, that has not only been my roommate in 2113, but also like a brother for the last 10 years is Jörgen Westlinder. I still remember our first encounter, when you forced me to face the fact that "i" and "e" was something that could be used in mathematics despite the fact that they are not numerals…thanks…

I also would like to mention a few persons that have been outstanding in their own ways; Olle, the miserable tennis player, our struggles on the tennis court give me the self-confidence I sometimes need. Apart from your excellent ball boy skills, you are a great friend; Uli, the German contribution at the department – even though your Swedish is starting to attain native standards, I don't think you have learned the Swedish equivalent to "nein"…at least not when I have asked for your assistance; the chronic capitalist Lars Jonsson, for answering all the "not so clever" questions during my first time at the department…later on, up until now, Ilia took over most of that responsibility; Christer for all the philosophic discussions; Jörgen Olsson for proof reading this thesis; and Herman "Nationalencyklopedin" Norde for obvious reasons. In the same breath I would like to thank Anders Hoel, particularly for your unselfish nature. I still think though, that you should have convinced Stina to let me give you that pain killing injection.

I would also like to thank the entire “Elektroniken” and especially the “Tunnfilmsgrupp”; Hans-Olof for waking my interest to this field during class, my closest co-author Gonzalo being my tutor in Spanish, Marianne Asplund for taking care of us, all the great friends outside the University; Anders & Malin, Takanen, Ture, Jontan, the table tennis guys in Riddaren BTK, Deffhåkan, Linder...your friendship is invaluable to me…

I would also like to thank Lena, for taking care of me, and for putting up with me, especially during the times when the 15 year old inside of me gets in control.

Last, but definitely not least, I would like to thank my family for always being there for me, and for supporting me in the decisions that I make…

Sent en natt till tonerna av U2,

Fredrik Engelmark

References

[1] B. Drafts, "Acoustic wave technology sensors" *IEEE Transactions on Microwave Theory and Techniques*, vol. 49, pp. 795-802, 2001.

[2] B. L. Olutade and W. D. Hunt, "Sensitivity analysis of a thin film bulk acoustic resonator ladder filter" presented at Proceedings of International Frequency Control Symposium, New York, NY, USA, 1997.

[3] J. F. Rosenbaum, "Resonators II: High Frequancy Performance and Advanced Applications" in *Bulk acoustic wave theory and devices*. USA: Artech House, 1988, pp. 436.

[4] F. S. Hickernell, "Measurement techniques for evaluating piezoelectric thin films" *IEEE Ultrasonics Symposium*, pp. 235-242, 1996.

[5] www.agilent.com

[6] http://www.icknowledge.com/history/history.html,

[7] J. F. Rosenbaum, "Piezoelectrically active acoustic propagation" in *Bulk acoustic wave theory and devices*. USA: Artech House, 1988, pp. 125.

[8] H. Nakahata, K. Higaki, A. Hachigo, S. Shikata, N. Fujimori, Y. Takahashi, T. Kajihara, and Y. Yamamoto, "High frequency surface acoustic wave filter using ZnO/diamond/Si structure" *Japanese Journal of Applied Physics, Part 1*, vol. 33, pp. 324-8, 1994.

[9] P. Wu, N. W. Emanetoglu, X. Tong, and Y. Lu, "Temperature compensation of SAW in ZnO/SiO_2/Si structure" presented at 2001 IEEE Ultrasonics Symposium. Proceedings. An International Symposium, Piscataway, NJ, USA, 2001.

[10] C. Caliendo, G. Saggio, P. Verardi, and E. Verona, "Piezoelectric AlN film for SAW device applications" *Ultrasonics Symposium*, pp. 249-252, 1993.

[11] C. Hyun, C. B. Vartuli, S. M. Donovan, C. R. Abernathy, S. J. Pearton, R. J. Shul, and C. Constantine, "Comparison of inductively coupled plasma Cl_2 and Cl_4H_2 etching of III-nitrides" *Journal of Vacuum Science & Technology A*, vol. 16, pp. 1631-5, 1998.

[12] H. Cho, C. B. Vartuli, C. R. Abernathy, S. M. Donovan, S. J. Pearton, R. J. Shul, and J. Han, "Cl_2-based dry etching of the AlGaInN system in inductively coupled plasmas" *Solid State Electronics*, vol. 42, pp. 2277-81, 1998.

[13] S. J. Pearton, "Dry etching processes for fabrication of QWIPs and other detector structures" *Proceedings of the SPIE The International Society for Optical Engineering*, vol. 2999, pp. 118-30, 1997.

[14] R. J. Shul, C. G. Willison, M. M. Bridges, J. Han, J. W. Lee, S. J. Pearton, C. R. Abernathy, J. D. MacKenzie, L. Zhang, and L. F. Lester, "Selective inductively coupled plasma etching of group-III nitrides in Cl_2- and BCl_3-based plasmas" *Journal of Vacuum Science & Technology A*, vol. 16, pp. 1621-6, 1998.

[15] S. A. Smith, C. A. Wolden, M. D. Bremser, A. D. Hanser, R. F. Davis, and W. V. Lampert, "Selective and non-selective etching of GaN, AlGaN, and AlN using an inductively coupled plasma" *Proceedings of the IEEE Twenty-Fourth International Symposium on Compound Semiconductors*, 1998, pp. 349-352.

[16] W. M. Yim, E. J. Stofko, P. J. Zanzucchi, J. I. Pankove, M. Ettenberg, and S. L. Gilbert, "Epitaxially grown AlN and its optical band gap" *Journal of Applied Physics*, vol. 44, pp. 292-6, 1973.

[17] S. Strite, M. E. Lin, and H. Morkoc, "Progress and prospects for GaN and the III-V nitride semiconductors" *Thin Solid Films*, vol. 231, pp. 197-210, 1993.

[18] G. Aylward and T. Findlay, "Properties of inorganic compounds" in *SI Chemical Data*, P. Storer, Ed. NY: John Wiley & Sons, 1971.

[19] H. Okano, N. Tanaka, K. Shibata, and S. Nakano, "GHz-band surface acoustic wave devices using aluminum nitride thin films deposited by electron cyclotron resonance dual ion-beam sputtering" *Japanese Journal of Applied Physics*, vol. 32, pp. 4052-4056, 1993.

[20] M. A. Dubois, P. Muralt, and V. Plessky, "BAW resonators based on aluminum nitride thin films" *1999 IEEE Ultrasonics Symposium Proceedings*, vol. 2, pp. 907-910, 1999.

[21] S. Tomabechi, K. Wada, S. Saigusa, H. Matsuhashi, H. Nakase, K. Masu, and K. Tsubouchi, "Development of high quality AlN epitaxial film for 2.4 GHz front-end SAW matched filter" *1999 IEEE Ultrasonics Symposium Proceedings*, vol. 2, pp. 263-267, 1999.

[22] A. H. Khan, J. M. Meese, E. J. Charlson, E. M. Charlson, T. Stacy, S. Khasavinah, T. Sung, G. Popovici, M. A. Prelas, J. E. Chamberlain, and H. W. White, "AlN on diamond thin films grown by chemical vapor deposition methods" *Proceedings of the SPIE The International Society for Optical Engineering*, vol. 2151, pp. 44-9, 1994.

[23] C. L. Aardahl, J. W. Rogers, Jr., H. K. Yun, Y. Ono, D. J. Tweet, and S.-T. Hsu, "Electrical properties of AlN thin films deposited at low temperature on Si(100)" *Thin Solid Films*, vol. 346, pp. 174-80, 1999.

[24] A. U. Ahmed, A. Rys, N. Singh, J. H. Edgar, and Z. J. Yu, "The electrical and compositional properties of AlN-Si interfaces" *Journal of the Electrochemical Society*, vol. 139, 1992.

[25] M. Razeghi, X. Zhang, P. Kung, A. Saxler, D. Walker, K. Y. Lim, and K. S. Kim, "Recent advances in III-nitride materials, characterization and device applications" *Proceedings of the SPIE - The International Society for Optical Engineering*, vol. 3179, pp. 2-11, 1997.

[26] C. C. Cheng, Y. C. Chen, H. J. Wang, and W. R. Chen, "Low-temperature growth of Aluminum Nitride thin films on Silicon by reactive radio frequency magnetron sputtering" *Journal of Vacuum Science & Technology A*, vol. 14, pp. 2238-2242, 1996.

[27] M. B. Assouar, O. Elmazria, L. L. Brizoual, and P. Alnot, "Reactive DC magnetron sputtering of aluminum nitride films for surface acoustic wave devices" *Diamond and Related Materials*, vol. 11, pp. 413-417, 2002.

[28] F. Brunet, F. Randriamora, A. Deneuville, P. Germi, B. Anterion, and M. Pernet, "Highly textured hexagonal AlN films deposited at low temperature by reactive cathodic sputtering" *Materials Science & Engineering B*, vol. 59, pp. 88-93, 1999.

[29] F. Engelmark, G. Fuentes, I. V. Katardjiev, A. Harsta, U. Smith, and S. Berg, "Synthesis of highly oriented piezoelectric AlN films by reactive sputter deposition" *Journal of Vacuum Science & Technology A*, vol. 18, pp. 1609-12, 2000.

[30] H. Maiwa and K. Okazaki, "Preparation of AlN thin films by reactive sputtering and optical emission spectroscopy during sputtering" *Ferroelectrics*, vol. 131, pp. 83-89, 1992.

[31] A. J. Noreika, M. H. Francombe, and S. A. Zeitman, "Dielectric properties of reactively sputtered films of aluminum nitride" *Journal of Vacuum Science and Technology*, vol. 6, pp. 194-7, 1969.

[32] R. Parsons, "Sputter Deposition Processes" in *Thin film processes II*, J. L. Vossen and W. Kern, Eds. CA, USA: Academic Press Limited, 1991, pp. 178.

[33] M. Ohring, "Plasma and ion beam processing of thin films" in *Materials science of thin films*. USA: Academic press, 2002, pp. 215.

[34] B. A. Westwood, "Physical Vapour Deposition" in *Material science of thin films*. USA: Academic Press, 2001, pp. 217.

[35] T. Nyberg, C. Nender, and S. Berg, "Composition control by current modulation in dc-reactive sputtering" *Journal of Vacuum Science & Technology A (Vacuum, Surfaces, and Films)*, vol. 16, pp. 1868-72, 1998.

[36] S. Berg, T. Nyberg, H.-O. Blom, and C. Nender, "Computer modeling as a tool to predict deposition rate and film composition in the reactive sputtering process" *Journal of Vacuum Science & Technology A (Vacuum, Surfaces, and Films)*, vol. 16, pp. 1277-85, 1998.

[37] T. Nyberg, P. Skytt, B. Galnander, C. Nender, J. Nordgren, and S. Berg, "Studies of reactive sputtering of multi-phase chromium nitride" *Journal of Vacuum Science & Technology A (Vacuum, Surfaces, and Films)*, vol. 15, pp. 248-52, 1997.

[38] J. Westlinder, Y. Zhang, F. Engelmark, G. Possnert, H.-O. Blom, J. Olsson, and S. Berg, "Simulation and dielectric characterization of reactive dc magnetron cosputtered $(Ta_2O_5)_{1-x}(TiO_2)_x$ thin films" *Journal of Vacuum Science & Technology B (Microelectronics and Nanometer Structures)*, vol. 20, pp. 855-61, 2002.

[39] S. Berg, T. Nyberg, H.-O. Blom, and C. Nender, "Modeling of the reactive sputtering process" in *Handbook of thin film process technology*, D. A. Glocker and S. Ismat Shah, Eds.: IOP, 1998, pp. A5.3:1-15.

[40] S. Berg, H.-O. Blom, T. Larsson, and C. Nender, "Modeling of reactive sputtering of compound materials" *Journal of Vacuum Science & Technology A*, vol. 5, pp. 202-7, 1987.

[41] S. Berg, H.-O. Blom, M. Moradi, C. Nender, and T. Larsson, "Process modeling of reactive sputtering" *Journal of Vacuum Science & Technology A*, vol. 7, pp. 1225-9, 1989.

[42] P. Carlsson, C. Nender, H. Barankova, and S. Berg, "Reactive sputtering using two reactive gases, experiments and computer modeling" *Journal of Vacuum Science & Technology A (Vacuum, Surfaces, and Films)*, vol. 11, pp. 1534-9, 1993.

[43] T. Larsson, H.-O. Blom, C. Nender, and S. Berg, "A physical model for eliminating instabilities in reactive sputtering" *Journal of Vacuum Science & Technology A*, vol. A6, pp. 1832-1836, 1987.

[44] S. Berg, T. Larsson, C. Nender, and H.-O. Blom, "Predicting thin-film stoichiometry in reactive sputtering" *Journal of applied physics*, vol. 63, pp. 887-891, 1987.

[45] L. Jonsson, "Experiments and modeling of thin film processes" Uppsala University, 1999.

[46] T. Nyberg, "Studies of the reactive sputtering process and CVD of diamond thin films" Uppsala University, 1997.

[47] S. Berg, T. Nyberg, H.-O. Blom, and C. Nender, "Modeling of the reactive sputtering process" in *Handbook of thin film process technology*, B. A. Westwood, Ed. USA: IoP, 1998, pp. A5.3:1-A5.3:15.

[48] J. A. Thornton, "Influence of apparatus geometry and deposition conditions on the structure and topography of thick sputtered coatings" *Journal of vacuum Science & Technology*, vol. 11, pp. 666-70, 1974.

[49] J. A. Thornton, J. Tabock, and D. W. Hoffman, "Internal stresses in metallic films deposited by cylindrical magnetron sputtering" *Thin Solid Films*, vol. 64, pp. 111-19, 1979.

[50] J. W. Coburn and H. F. Winters, "Ion- and electron-assisted gas-surface chemistry-an important effect in plasma etching" *Journal of Applied Physics*, vol. 50, pp. 3189-96, 1979.

[51] M. B. Assouar, O. Elmazria, R. J. Rioboo, F. Sarry, and P. Alnot, "Modelling of SAW filter based on ZnO/diamond/Si layered structure including velocity dispersion" *Applied Surface Science*, vol. 164, pp. 200-4, 2000.

[52] J. Koskela, V. P. Plessky, and M. M. Salomaa, "SAW/LSAW COM parameter extraction from computer experiments with harmonic admittance of a periodic array of electrodes" *IEEE Transactions on Ultrasonics, Ferroelectrics and Frequency Control*, vol. 46, pp. 806-16, 1999.

[53] V. Plesky and J. Koskela, "Coupling of modes analysis of SAW devices" *International Journal of High Speed Electronics and Systems*, vol. 10, pp. 867, 2000.

[54] P. V. Wright, "Analysis and design of low-loss SAW devices with internal reflections using coupling-of-modes theory" in *IEEE 1989 Ultrasonics Symposium Proceedings*, vol. vol.1. New York, NY, USA: IEEE, 1989, pp. 141-52.

[55] V. M. Yantchev and V. L. Strashilov, "Coupling-of-modes analysis of STW resonators including loss mechanism" *IEEE Transactions on Ultrasonics, Ferroelectrics and Frequency Control*, vol. 49, pp. 331-6, 2002.

[56] S. Datta, *Surface Acoustic Wave Devices*. New Jersey, USA: Prentice-Hall, 1986.

[57] J. F. Rosenbaum, in *Bulk acoustic wave theory and devices*. USA: Artech House, 1988.

[58] H. Nowotny, E. Benes, and M. Schmid, "Layered piezoelectric resonators with an arbitrary number of electrodes (general one-dimensional treatment)" *Journal of the Acoustical Society of America*, vol. 90, pp. 1238-45, 1991.

[59] H. Nowotny and E. Benes, "General one-dimensional treatment of the layered piezoelectric resonator with two electrodes" *Journal of the Acoustical Society of America*, vol. 82, pp. 513-21, 1987.

[60] J. F. Rosenbaum, "Resonators I: Basic Theory" in *Bulk acoustic wave theory and devices*. USA: Artech House, 1988, pp. 397.

[61] S. Maniv, C. J. Miner, and W. D. Westwood, "Transparent conducting zinc oxide and indium-tin oxide films prepared by modified reactive planar magnetron sputtering" *Journal of Vacuum Science & Technology A*, vol. 1, pp. 1370-5, 1983.

[62] G. Este and W. D. Westwood, "Reactive deposition of low loss Al_2O_3 optical waveguides by modified DC planar magnetron sputtering" *Journal of Vacuum Science & Technology A*, vol. 2, pp. 1238-47, 1984.

[63] T. Hata, K. Sasaki, and Y. Ichikawa, "Yttria-stabilized zirconia (YSZ) heteroepitaxially grown on Si substrates by reactive sputtering" *Vacuum*, vol. 59, pp. 381-9, 2000.

[64] T. Hata, S. Nakano, Y. Masuda, K. Sasaki, Y. Haneda, and K. Wasa, "Heteroepitaxial growth of YSZ films on Si(100) substrate by using new metallic mode of reactive sputtering" *Vacuum*, vol. 51, pp. 583-90, 1998.

[65] Y.-J. Yong and J.-Y. Lee, "Characteristics of hydrogeated Aluminum Nitride films prepared by radio frequency reactive sputtering and their applications to surface acoustic wave devices" *Journal of Vacuum Science & Technology A*, vol. 15, pp. 390-393, 1996.

[66] K. Jagannadham, A. K. Sharma, Q. Wei, R. Kalyanraman, and J. Narayan, "Comparison of AlN films synthesized by pulsed laser ablation and magnetron sputtering techniques" presented at Thin-Films-Stresses and Mechanical Properties VII. Symposium, Warrendale, PA, USA, 1998.

[67] H. L. Kao, P. J. Shih, and C.-H. Lai, "The study of preferred orientation growth of aluminum nitride thin films on ceramic and glass substrates" *Japanese Journal of Applied Physics, Part 1*, vol. 38, pp. 1526-9, 1999.

[68] K.-S. Kao, C.-C. Cheng, and Y.-C. Chen, "Synthesis of c-axis-oriented aluminum nitride films by reactive RF magnetron sputtering for surface acoustic wave" *Japanese Journal of Applied Physics, Part 1*, vol. 40, pp. 4969-73, 2001.

[69] C. Caliendo, A. Cimmino, P. Imperatori, and E. Verona, "Optimization of the sputtering deposition parameters of highly oriented piezoelectric AlN films" in *2000 IEEE Ultrasonics Symposium. Proceedings*, pp. 345-8.

[70] Y.-J. Yong, Y.-S. Kang, P. S. Lee, and J.-Y. Lee, "Fabrication of c-axis oriented ZnO/AlN thin films prepared by radio frequency reactive sputtering and development of ZnO/AlN layered structure surface acoustic wave devices" *Journal of Vacuum Science & Technology B*, vol. 20, pp. 42-6, 2002.

[71] R. S. Naik, R. Reif, J. J. Lutsky, and C. G. Sodini, "Low-temperature deposition of highly textured aluminum nitride by direct current magnetron sputtering for applications in thin-film resonators" *Journal of the Electrochemical Society*, vol. 146, pp. 691-6, 1999.

[72] M. Ishihara, S. J. Li, H. Yumoto, K. Akashi, and Y. Ide, "Control of preferential orientation of AlN films prepared by the reactive sputtering method" *Thin Solid Films*, vol. 316, pp. 152-157, 1998.

[73] G. L. Huffman, D. E. Fahnline, R. Messier, and L. J. Pilione, "Stress dependence of reactively sputtered aluminum nitride thin films on sputtering parameters" *Journal of Vacuum Science & Technology A*, vol. 7, pp. 2252-5, 1989.

[74] K. Tominaga, T. Ao, I. Mori, K. Kusaka, and T. Hanabusa, "Gas pressure dependence of AlN film properties in alternating sputtering system" *Japanese Journal of Applied Physics, Part 1*, vol. 35, pp. 4972-4975, 1996.

[75] H. Fusstetter, A. Schnegg, D. Graf, H. Kirschner, M. Brohl, and P. Wagner, "Impact of chemomechanical polishing on the chemical composition and morphology of the silicon surface" presented at Ultraclean Semiconductor Processing Technology and Surface Chemical Cleaning and Passivation. Symposium, Pittsburgh, PA, USA, 1995.

[76] K. Kaya, H. Takahashi, Y. Shibata, Y. Kanno, and T. Hirai, "Synthesis and surface acoustic wave properties of AlN thin films fabricated on (001) and (110) Sapphire substrates using chemical vapour deposition of $AlCl_3$-NH_3 system" *Japanese Journal of Applied Physics, Part 1*, vol. 36, pp. 2837-2842, 1997.

[77] K. Kaya, Y. Kanno, H. Takahashi, Y. Shibata, and T. Hirai, "Synthesis of AlN thin films on Sapphire substrates by chemical vapour deposition of $AlCl_3$-NH_3 system and surface acoustic wave properties" *Japanese Journal of Applied Physics, Part 1*, vol. 35, pp. 2782-2787, 1996.

[78] M. Albrecht, I. P. Nikitina, A. E. Nikolaev, Y. V. Melnik, V. A. Dmitriev, and H. P. Strunk, "Dislocation reduction in AlN and GaN bulk crystals grown by HVPE" *Physica Status Solidi A*, vol. 176, pp. 453-8, 1999.

[79] T. Shiosaki, T. Yamamoto, T. Oda, K. Harada, and A. Kawabata, "Low temperature growth of piezoelectric films by RF reactive planar magnetron sputtering" *Japanese Journal of Applied Physics*, vol. 20, pp. 149-52, 1981.

[80] S. Uchiyama, Y. Ishigami, M. Ohta, M. Niigaki, H. Kan, Y. Nakanishi, and T. Yamaguchi, "Growth of AlN films by magnetron sputtering" *Journal of Crystal Growth*, vol. 189-190, pp. 448-51, 1998.

[81] D. W. Hoffman and J. A. Thronton, "The compressive stress transition in Al, V, Zr, Nb and W metal films sputtered at low working pressures" *Thin Solid Films*, vol. 45, pp. 387-96, 1977.

[82] D. W. Hoffman and J. A. Thornton, "Internal stresses in sputtered chromium" *Thin Solid Films*, vol. 40, pp. 355-63, 1977.

[83] K. S. Stevens, M. Kinniburgh, A. F. Schwartzman, A. Ohtani, and R. Beresford, "Demonstration of a silicon field-effect transistor using AlN as the gate dielectric" *Applied Physics Letters*, vol. 66, pp. 3179-81, 1995.

[84] V. Dimitrova, D. Manova, and E. Valcheva, "Optical and dielectric properties of DC magnetron sputtered AlN thin films correlated with deposition conditions" *Materials Science & Engineering B*, vol. B68, pp. 1-4, 1999.

[85] M. A. Dubois and P. Muralt, "Properties of aluminum nitride thin films for piezoelectric transducers and microwave filter applications" *Applied Physics Letters*, vol. 74, pp. 3032-4, 1999.

[86] R. F. Cava, W. F. Peck, Jr., and J. J. Krajewski, "Enhancement of the dielectric constant of Ta_2O_5 through substitution with TiO_2" *Nature*, vol. 377, pp. 215-17, 1995.

[87] S. W. Park, Y. K. Baek, J. Y. Lee, C. O. Park, and H. B. Im, "Effects of annealing conditions on the properties of tantalum oxide films on silicon substrates" *Journal of Electronic Materials*, vol. 21, pp. 635-9, 1992.

[88] S.-D. Cho and K.-W. Paik, "Study on the amorphous Ta_2O_5 thin film capacitors deposited by dc magnetron reactive sputtering for multichip module applications" *Materials Science & Engineering B*, vol. B67, pp. 108-12, 1999.

[89] R. J. Shul, L. Zhang, C. G. Willison, J. Han, S. J. Pearton, J. Hong, C. R. Abernathy, and L. F. Lester, "Group-III nitride etch selectivity in BCl_3/Cl_2 ICP plasmas" in *MRS Internet J. Nitride Semicond. Res. 4S1, G8.1*, 1999, pp. 1028.

[90] D. M. Manos and D. L. Flamm, "Plasma-Materials Interactions" in *Plasma etching*, O. Auciello and D. L. Flamm, Eds.: Academic Press, Inc., 1989.

[91] H. F. Winters, "Etch products from the reaction on Cl_2 with Al(100) and Cu(100) and XeF_2 with W(111) and Nb" *Journal of Vacuum Science & Technology B*, vol. 3, pp. 9-15, 1985.

[92] S. A. Smith, C. A. Wolden, M. D. Bremser, A. D. Hanser, R. F. Davis, and W. V. Lampert, "High rate and selective etching of GaN, AlGaN, and AlN using an inductively coupled plasma" *Applied Physics Letter*, vol. 71, pp. 3631-3, 1997.

[93] http://www.tydex.ru/materials/materials2/crystal_quartz.html,

[94] J. D. Larson, III, R. C. Ruby, and P. Bradley, "Bulk Acoustic Resonator with improved lateral mode suppression" in *European patent applications*, 2000, pp. 7.

[95] J. D. Larson, III, J. D. Ruby, III, R. C. Bradley, J. Wen, S.-L. Kok, and A. Chien, "Power handling and temperature coefficient studies in FBAR duplexers for the 1900 MHz PCS band" presented at 2000 IEEE Ultrasonics Symposium. Proceedings. An International Symposium, Piscataway, NJ, USA, 2000.

[96] H. M. Liaw and F. S. Hickernell, "The characterization of sputtered polycrystalline aluminum nitride on silicon by surface acoustic wave measurements" *IEEE Transactions on Ultrasonics, Ferroelectrics and Frequency Control*, vol. 42, pp. 404-9, 1995.

[97] F. S. Hickernell and H. M. Liaw, "The structural and acoustic properties of sputtered Aluminum Nitride on Silicon" *International symposium on applications of ferroelectrics*, vol. 9, pp. 543-546, 1994.

[98] S.-H. Lee, H.-H. Jeong, S.-B. Bae, H.-C. Choi, J.-H. Lee, and Y.-H. Lee, "Epitaxially grown GaN thin-film SAW filter with high velocity and low insertion loss" *IEEE Transactions on Electron Devices*, vol. 48, pp. 524-9, 2001.